Results of wake simulations at the Horns Rev I and Lillgrund wind farms using the modified Park model

Peña, Alfredo; Réthoré, Pierre-Elouan; Hasager, Charlotte Bay; Hansen, Kurt Schaldemose

Publication date:
2013

Document Version
Publisher's PDF, also known as Version of record

Results of wake simulations at the Horns Rev I and Lillgrund wind farms using the modified Park model

DTU Wind Energy E-Report

Alfredo Peña, Pierre-Elouan Réthoré,
Charlotte B. Hasager, and Kurt S. Hansen

DTU Wind Energy-E-Report-0026(EN)
October 2013

DTU Wind Energy
Department of Wind Energy

DTU Wind Energy-E-Report-0026(EN)

Results of wake simulations at the Horns Rev I and Lillgrund wind farms using the modified Park model

Alfredo Peña, Pierre-Elouan Réthoré, Charlotte B. Hasager, and Kurt S. Hansen

EERA DTOC
THE EUROPEAN ENERGY RESEARCH ALLIANCE
DESIGN TOOLS FOR OFFSHORE WIND FARM CLUSTER

IEA Wind Task 31 Wakebench

DTU Wind Energy
Department of Wind Energy

DTU

**DTU Wind Energy, Risø Campus,
Technical University of Denmark, Roskilde, Denmark**

October 2013

Author: Alfredo Peña, Pierre-Elouan Réthoré, Charlotte B. Hasager, and Kurt S. Hansen
Title: Results of wake simulations at the Horns Rev I and Lillgrund wind farms using the modified Park model
Department: DTU Wind Energy

DTU Wind Energy-E-Report-0026(EN)
October 21, 2013

ISSN:
ISBN:
978-87-92896-38-4

Abstract (max. 2000 char)

This document reports on the results of the wake simulations performed at both the Horns Rev I and Lillgrund offshore wind farms using the modified Park model for the benchmark cases established under the project EERA-DTOC and the IEC Wind Task Wakebench. It also illustrates the comparison between model simulations and the data. The latter were first independently analyzed by Kurt Hansen and kindly delivered to us after the results of the models' benchmarks were publicly released. For Horns Rev I, the simulations agree very well with the observations, particularly when the simulation results are post-processed to partly take into account the wind direction uncertainty and when the wake decay coefficient is estimated either as function of the roughness, height, and atmospheric stability or turbulence intensity. For Lillgrund, the trends of the simulations and the observations are generally the same, although the agreement is not as good as for the Horns Rev I case. When taking into account direction uncertainty, an improvement is found as well as when using the wake decay coefficient parametrization

Contract no:
2011-/no.282797

Project no:
43077

Sponsorship:
FP7-Energy

Cover:

Pages: 40
Tables: 25
Figures: 36
References: 17

Technical University of Denmark
Frederiksborgvej 399
4000 Roskilde
Denmark
Tel. +4546775024
bcar@dtu.dk
www.vindenergi.dk

Contents

Page

1 Model description, post-processing and definitions **5**
1.1 Model description . . . 5
1.1.1 Wake decay coefficient k_w . . . 5
1.2 Post-processing . . . 6
1.3 Definitions . . . 7

2 Wind farm description **8**
2.1 Horns Rev I . . . 8
2.2 Lillgrund . . . 8

3 Horns Rev I cases **10**
3.1 Flow sector variation . . . 10
3.1.1 Wind direction $270 \pm 0°$ . . . 10
3.1.2 Wind direction $270 \pm 2.5°$ . . . 11
3.1.3 Wind direction $270 \pm 7.5°$ . . . 11
3.1.4 Wind direction $270 \pm 15°$ . . . 13
3.2 Atmospheric stratification . . . 14
3.2.1 Unstable case . . . 14
3.2.2 Neutral case . . . 15
3.2.3 Stable case . . . 15
3.3 Turbulence intensity . . . 15
3.3.1 Flow sector $250 - 290°$ and 7D spacing . . . 15
3.3.2 Flow sector $90 \pm 2.5°$ and 7D spacing . . . 16
3.3.3 Flow sector $132 \pm 2.5°$ and 10.4D spacing . . . 17
3.4 Spacing . . . 19
3.4.1 7D spacing and $270 \pm 5°$ . . . 19
3.4.2 9.4D spacing and $221 \pm 5°$ . . . 20
3.4.3 10.4**D** spacing and $132 \pm 5°$ . . . 21
3.5 Park efficiency . . . 23

4 Lillgrund cases **26**
4.1 Sector variation . . . 26
4.1.1 3.3D spacing $120°$ . . . 26
4.1.2 4.3D spacing $222°$ . . . 26
4.2 Speed recovery . . . 30
4.2.1 3.3D spacing $120°$ – 2 missing turbines . . . 30
4.2.2 4.3D spacing $222°$ – 1 missing turbine . . . 32
4.3 Turbulence intensity . . . 34
4.3.1 Flow sector $120 \pm 2.5°$ and 3.3D spacing . . . 34
4.3.2 Flow sector $222 \pm 2.5°$ and 4.3D spacing . . . 35
4.4 Park efficiency . . . 36

5 Summary and conclusions **38**

Acknowledgments **39**

References **40**

1 Model description, post-processing and definitions

1.1 Model description

We use a modified version of the Park wake model (Katic et al., 1986) applied in the Wind Atlas Analysis and Application Program (WAsP) (Mortensen et al., 2007). This modified version mainly differs from that in WAsP in that it does not take into account the effects of the ground creating "underground" wakes and so it only takes into account "real" shading rotors both directly upstream and sideways.

The Park wake model is based on the wake model by Jensen (1983), who by mass-conservation means (see Fig. 1) derived an equation for the velocity immediately before a wake-affected turbine, u_1,

$$u_1 = u_{free}\left[1 - \frac{a}{(1 + k_w\ x/r_r)^2}\right], \tag{1}$$

where u_{free} is the upstream undisturbed wind speed, a the induction factor ($a = 1-\sqrt{1-C_t}$), k_w the wake decay coefficient, x the distance, and r_r the turbine's rotor radius.

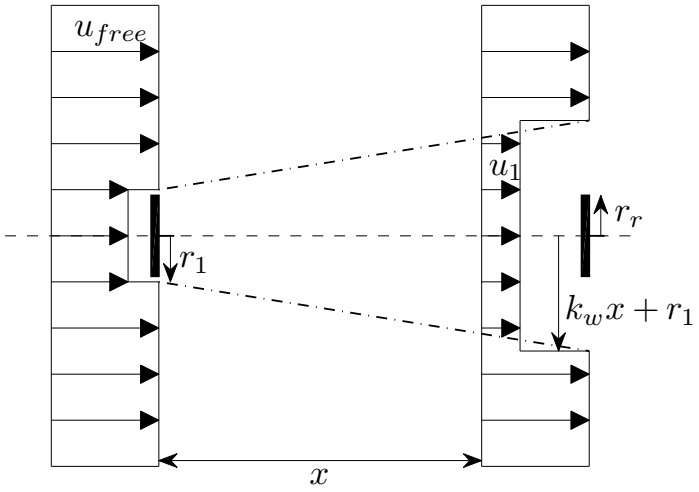

Figure 1: The wake model of Jensen (1983)

The contributions of Katic et al. (1986) to Jensen (1983) were mainly two: 1) to suggest, based on wind tunnel results, that the square of the total wake deficit should be the sum of the square of all contributing wake deficits (e.g. for the first turbine the wake deficit is given as 1-u_1/u_{free}) and 2) to introduce the effect of the underground rotors.

We implemented the model in a Matlab script, which is very fast; for a specific wind direction and wind speed a wind farm of 80 wind turbines is modeled in less than 37 ms. Any kind of wind farm sizes and wind turbine model types are permitted, although it does not allow to have more than one turbine type yet.

1.1.1 Wake decay coefficient k_w

The results of the simulations are very dependent on k_w as the wind speed recuperates faster and the wake becomes wider for higher than lower k_w values. Neither Jensen (1983) nor Katic

et al. (1986) suggested a value for k_w. Frandsen (1992) mentioned that by semi-empirical means

$$k_w = \frac{0.5}{\ln(h/z_o)}, \tag{2}$$

where h is the turbine's hub height and z_o is the surface roughness. Using $h = 70$ m and $z_o = 0.0002$ m, $k_w = 0.0392$, which is already a lower value compared to that of 0.0500 recommended in WAsP when performing energy yields offshore. In Peña and Rathmann (2013) it was already found that the WAsP recommended values were much higher than those found when adjusting the Park model computed for an infinite wind farm to an infinite boundary-layer model.

We argue that k_w is related to the atmospheric turbulence flow characteristics and suggest

$$k_w = \frac{u_*}{u_h}, \tag{3}$$

where u_* is the friction velocity and u_h the hub-height wind speed as in Peña and Rathmann (2013) and Peña et al. (2013). Since the inflow (free) conditions are normally given/known, we assume $k_w = u_{*free}/u_{hfree}$, which allows us – by using Monin-Obukhov similarity theory (Monin and Obukhov, 1954) – to express k_w as function of hub height, atmospheric static stability and roughness,

$$k_w = \frac{\kappa}{\ln(h/z_o) - \psi_m(h/L)}, \tag{4}$$

where κ is the von Kármán constant (0.4) and ψ_m is the correction due to stability of the logarithmic wind profile, which is dependent of both the height and the Obukhov length L. For example, under neutral conditions $\psi_m(h/L) = 0$ and thus Eq. (4) becomes close to the suggestion by Frandsen (1992). Similarly, we can also express k_w as function of turbulence intensity, $\mathrm{TI} = \sigma_u/u$, where σ_u is the wind speed standard deviation. Assuming $\sigma_u = 2.5u_*$ as in Panofsky and Dutton (1984),

$$k_w = 0.4\ \mathrm{TI}. \tag{5}$$

1.2 Post-processing

Simulations, unless otherwise stated, are performed for a single inflow hub-height wind speed (given by the specific case) and for a wide range of wind directions (normally $\pm 45°$) with a resolution of $0.1°$. For example, for a "$270°$ case" the simulations are performed in the interval $[225 : 0.1 : 315]°$.

As we compare our simulations with data averaged (within 10 min) under some range of wind directions (typically $\pm 5°$), we assume (because we do not know more about the data) that observations within that direction range were equally observed at half degree steps. So for a theoretical $270 \pm 5°$ case, we assume that 10-min data are observed with wind directions $[265 : 0.5 : 275]°$.

Further, we partly take into account the wind direction uncertainty as in Gaumond et al. (2013) and Peña et al. (2013), by assuming that within a 10-min period, the additional wind direction uncertainty distributes as a Gaussian distribution with a width characterized by the standard deviation σ. The procedure is then to take each of the "assumed observed" 10-min wind directions θs (see paragraph above), extract the simulations correspondent to the range $[\theta - 3\sigma, \theta + 3\sigma]$ and then weight each simulation using the normal distribution function. For each "assumed observed" 10-min wind direction and speed deficit, there is therefore a single simulated wind speed deficit derived from $2 \times 3\sigma/0.1$ Gaussian-weighted simulations. Then we average the gaussian-weighted single simulated wind speed deficits within the range used given by the benchmark.

1.3 Definitions

The results of both simulations and the SCADA analysis are given by estimating the power deficit defined as,

$$\text{Power deficit} = 1 - P_i/P_u, \tag{6}$$

where P_i is the power of a specific turbine i downstream the "undisturbed-free" turbine with power P_u.

In the case of efficiency, this is given as,

$$\text{Efficiency} = \frac{\Sigma_i P_i}{N\ P_u}, \tag{7}$$

where N is the number of turbines in the wind farm. This has been adopted following the analysis in Hansen et al. (2012).

2 Wind farm description

2.1 Horns Rev I

Horns Rev I is an offshore wind farm about 12-17 km from the Danish west coast. It has been extensively described and the meteorological and SCADA data utilized in the literature (Peña et al., 2008, 2009; Hansen et al., 2012; Peña and Hahmann, 2012; Gaumond et al., 2013). The wind farm consists of 80 Vestas V80 2 MW pitch controlled wind turbines with hub heights at 70 m above mean sea level (AMSL) and rotor diameters (D) of 80 m. The wind farm's columns (10) are defined nearly southwards, whereas the rows (8) are aligned eastwards as seen from Fig. 2 (i.e. row 1 comprises turbines 01, 11,..., 91). Figure 3 illustrates the power and thrust curves of the Vestas machine used in Horns Rev I.

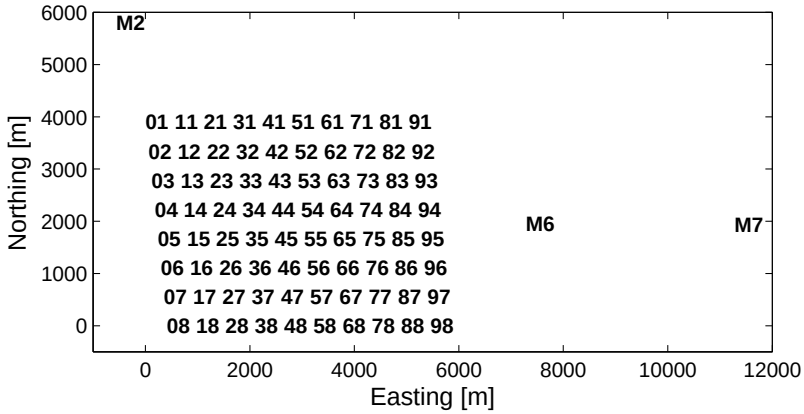

Figure 2: The Horns Rev I offshore wind farm and the meteorological masts M2, M6, and M7

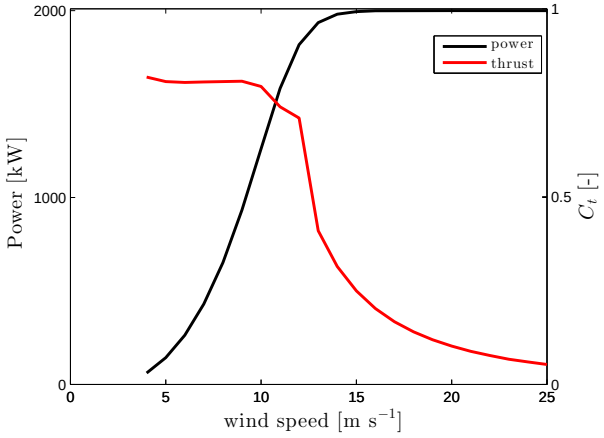

Figure 3: Power and thrust curves of the Vestas V80 2 MW turbine

2.2 Lillgrund

Lillgrund is an offshore wind farm in Øresund about 6–8 km from the Swedish west coast and south of Malmö, Sweden. The wind farm consists of 48 Siemens SWT-2.3-93 2.3 MW pitch controlled, variable speed wind turbines with hub heights at 65 m AMSL and D $= 92.6$ m. The turbines are labeled with letters and numbers; there are 8 rows northwestwards (letters) and 8 rows southwestwards (numbers) as seen from Fig. 4. Figure 5 illustrates the power and

thrust curves of the Siemens machine used in Lillgrund.

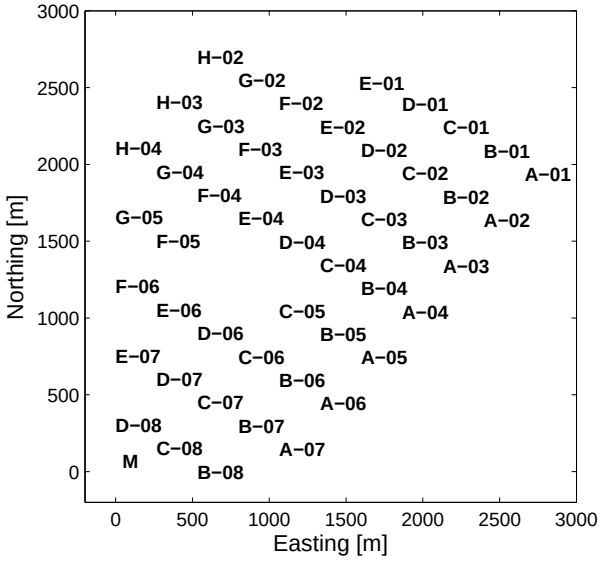

Figure 4: The Lillgrund offshore wind farm and the meteorological mast M

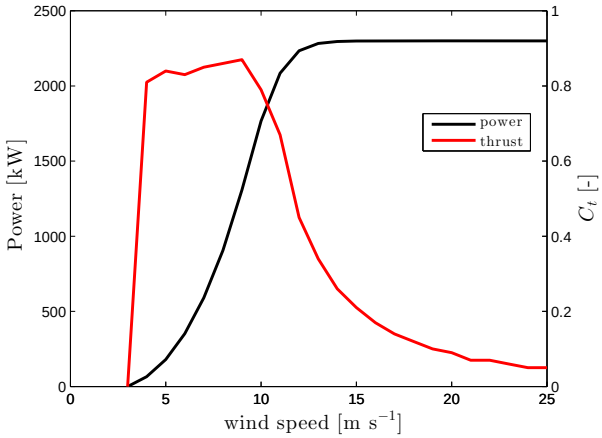

Figure 5: Power and thrust curves of the Siemens SWT-2.3-93 turbine

3 Horns Rev I cases

The simulations are, unless otherwise stated, performed with two k_w-values: 0.0500 (WAsP recommended) and $k_w = 0.0313$ assuming $u_{hfree} = 8$ m s^{-1}. The latter results by evaluating Eq. (4) with the Vestas turbine specifications in Section 2.1 using $z_o = 0.0002$ m (Peña and Gryning, 2008) and $\psi_m(h/L) = 0$ (Peña, 2009). Further, results using $\sigma = 0°$ and $\sigma = X°$, with X varying upon the case, are also computed. Observations and data treatment are described in Hansen (2013a).

3.1 Flow sector variation

Figure 6 illustrates the row used to extract SCADA data and simulations results for all flow sector variation cases (row 7). The wind direction is $270°$ and the different cases corresponds to broader/narrower wind direction sizes.

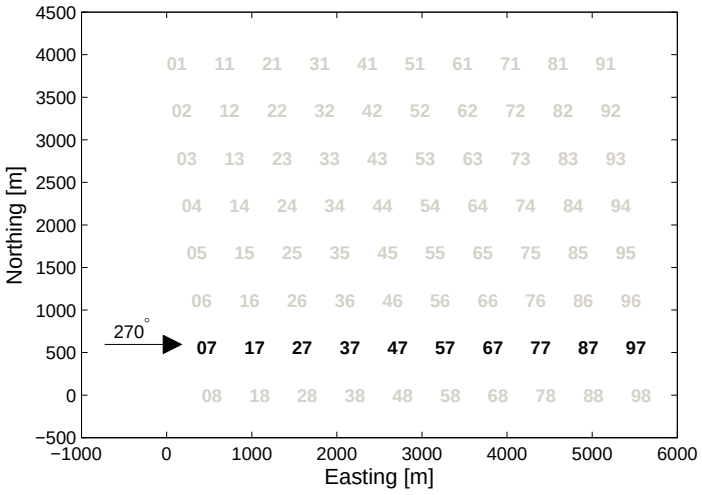

Figure 6: Schematics of the turbines (row 7) analyzed for all flow sector variation and atmospheric stability cases and first 7D spacing case

Sometimes the SCADA analysis for this type of cases is performed by averaging the power deficits from rows 2–7. Negligible differences from the simulations were found for all flow sector variation cases when averaging rows 2–7 compared to take row 7 alone (so the results for the latter case are shown only).

3.1.1 Wind direction $270 \pm 0°$

Figure 7 and Table 1 show the results for this case with $k_w = 0.0313$ and $k_w = 0.0500$ and with $\sigma = 0°$ and $\sigma = 8°$. The latter value for σ was selected as we expect that when taking very narrow wind direction sizes, the effects of the wind direction uncertainty will become higher. Gaumond et al. (2013) showed that for a particular 10-min interval of wind directions, with a mean close to $270°$, its distribution was very close to Gaussian with $\sigma \approx 3°$.[1] But this natural variation of wind direction is just one of the causes of the wind direction uncertainty; other are yaw misalignment both between turbine and wind and between turbines and "real" wind direction differences along the wind farm.

[1] For a given wind speed and turbulence intensity value

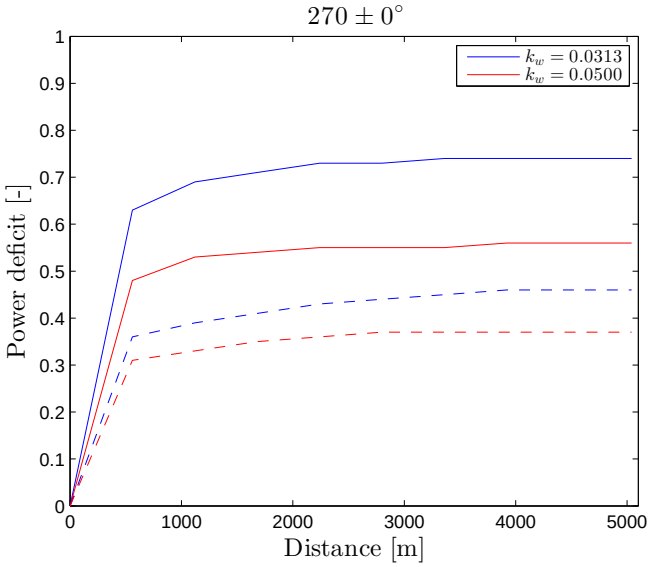

Figure 7: Results for the wind direction $270 \pm 0°$ test case. Solid and dashed lines correspond to $\sigma = 0°$ and $\sigma = 8°$, respectively

Table 1: Results for the wind direction $270 \pm 0°$ test case

distance [m] Model run	0	560	1120	1680	2240	2800	3360	3920	4480	5040
$\sigma = 0°$ $k_w = 0.0313$	0.00	0.63	0.69	0.71	0.73	0.73	0.74	0.74	0.74	0.74
$\sigma = 0°$ $k_w = 0.0500$	0.00	0.48	0.53	0.54	0.55	0.55	0.55	0.56	0.56	0.56
$\sigma = 8°$ $k_w = 0.0313$	0.00	0.36	0.39	0.41	0.43	0.44	0.45	0.46	0.46	0.46
$\sigma = 8°$ $k_w = 0.0500$	0.00	0.31	0.33	0.35	0.36	0.37	0.37	0.37	0.37	0.37

Higher power deficits are observed for the lower k_w-value as expected. As there is no direction size, the power deficit at Horns Rev I is expected to be highest at $270°$, since, e.g. the wake of turbine 07 directly hits 17. When assuming a direction uncertainty we account for directions other than $270°$ (aligned with turbines 07 and 17) and thus the power deficit becomes lower.

3.1.2 Wind direction $270 \pm 2.5°$

Figure 8 and Table 2 show the results for this case with $k_w = 0.0313$ and $k_w = 0.0500$ and with $\sigma = 0°$ and $\sigma = 8°$. The differences between this and the $270 \pm 0°$ are minimal as the direction size is very small.

3.1.3 Wind direction $270 \pm 7.5°$

Figure 9 and Table 3 show the results for this case with $k_w = 0.0313$ and $k_w = 0.0500$ and with $\sigma = 0°$ and $\sigma = 8°$. The differences between this and the two previous cases are well noticeable as the power deficits are much lower for the $\sigma = 0°$ as the direction size is bigger and so the upstream wakes are not always hitting directly those downstream. It is interesting to see that the differences for the $\sigma = 8°$ simulation and the previous case are rather low.

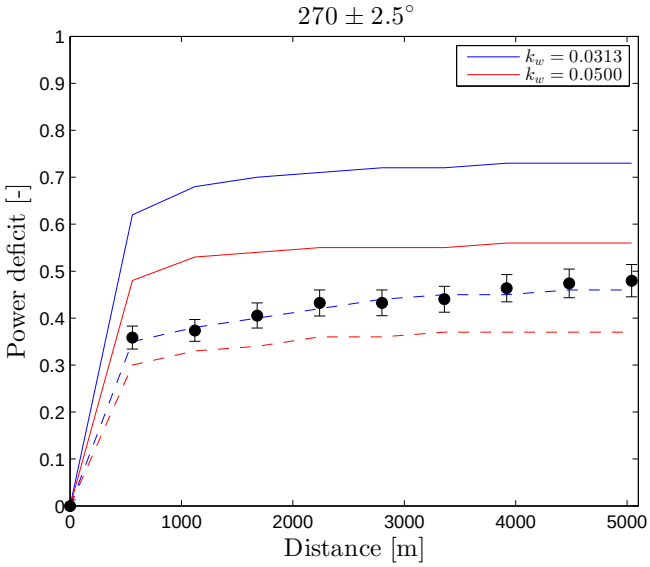

Figure 8: Results for the wind direction $270 \pm 2.5^\circ$ test case. Solid and dashed lines correspond to $\sigma = 0^\circ$ and $\sigma = 8^\circ$, respectively. Observations are shown in markers and the error bars provide their uncertainty

Table 2: Results for the wind direction $270 \pm 2.5^\circ$ test case

distance [m] Model run	0	560	1120	1680	2240	2800	3360	3920	4480	5040
$\sigma = 0^\circ$ $k_w = 0.0313$	0.00	0.62	0.68	0.70	0.71	0.72	0.72	0.73	0.73	0.73
$\sigma = 0^\circ$ $k_w = 0.0500$	0.00	0.48	0.53	0.54	0.55	0.55	0.55	0.56	0.56	0.56
$\sigma = 8^\circ$ $k_w = 0.0313$	0.00	0.35	0.38	0.40	0.42	0.44	0.45	0.45	0.46	0.46
$\sigma = 8^\circ$ $k_w = 0.0500$	0.00	0.30	0.33	0.34	0.36	0.36	0.37	0.37	0.37	0.37

This is mainly because we already account for a large part of the wind direction uncertainty when using such broader direction sizes.

Table 3: Results for the wind direction $270 \pm 7.5^\circ$ test case

distance [m] Model run	0	560	1120	1680	2240	2800	3360	3920	4480	5040
$\sigma = 0^\circ$ $k_w = 0.0313$	0.00	0.46	0.48	0.49	0.50	0.50	0.50	0.51	0.51	0.51
$\sigma = 0^\circ$ $k_w = 0.0500$	0.00	0.40	0.42	0.43	0.43	0.44	0.44	0.44	0.44	0.44
$\sigma = 8^\circ$ $k_w = 0.0313$	0.00	0.32	0.35	0.38	0.40	0.42	0.43	0.43	0.43	0.44
$\sigma = 8^\circ$ $k_w = 0.0500$	0.00	0.27	0.30	0.32	0.34	0.34	0.35	0.35	0.35	0.35

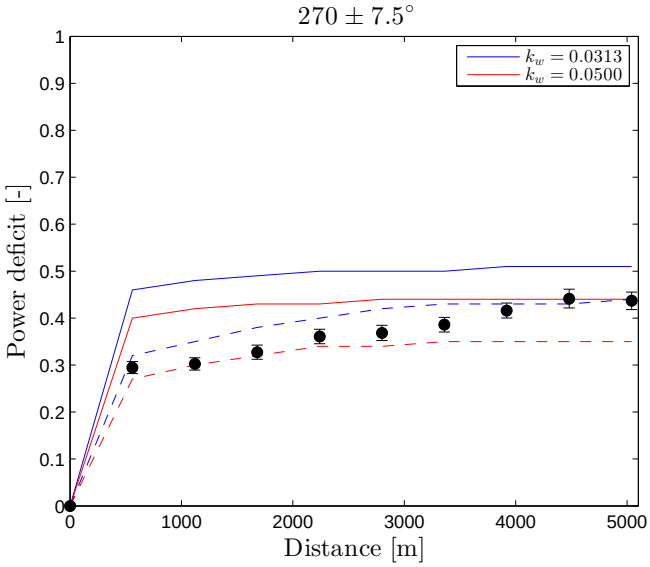

Figure 9: Results for the wind direction $270 \pm 7.5^\circ$ test case. Solid and dashed lines correspond to $\sigma = 0^\circ$ and $\sigma = 8^\circ$, respectively. Observations are shown in markers and the error bars provide their uncertainty

3.1.4 Wind direction $270 \pm 15^\circ$

Figure 10 and Table 4 show the results for this case with $k_w = 0.0313$ and $k_w = 0.0500$ and with $\sigma = 0^\circ$ and $\sigma = 8^\circ$. Here the simulations using $\sigma = 8^\circ$ even show (most of the time) higher power deficits than without direction uncertainty. Due to the higher direction size the power deficits are lowest compared to the previous cases. One interesting feature in the simulations without direction uncertainty is that turbines 17, 27, and 37. This is mostly due to the effect of turbines 06 and 08 on these turbines as for directions close to the limits of the interval, the wakes of 06 and 08 hit turbines 47 and downstream. When taking the direction uncertainty into account, wakes from turbines 06 and 08 also affect 17, 27, and 37.

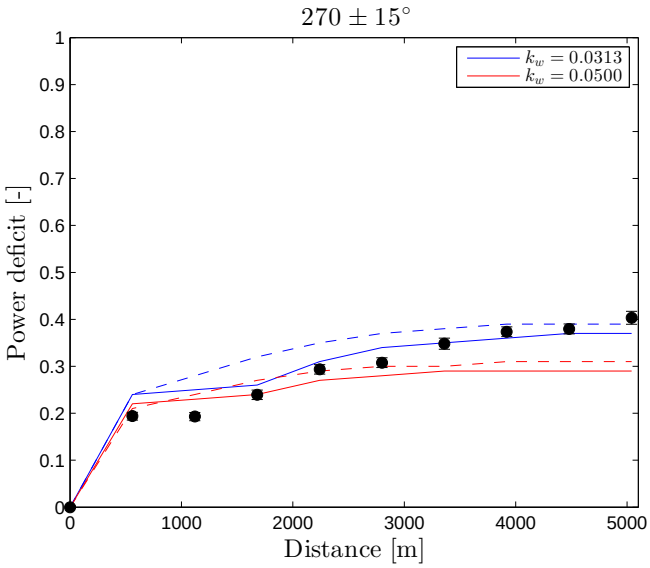

Figure 10: Results for the wind direction $270 \pm 15^\circ$ test case. Solid and dashed lines correspond to $\sigma = 0^\circ$ and $\sigma = 8^\circ$, respectively. Observations are shown in markers and the error bars provide their uncertainty

Table 4: Results for the wind direction $270 \pm 15^\circ$ test case

distance [m] Model run	0	560	1120	1680	2240	2800	3360	3920	4480	5040
$\sigma = 0^\circ$ $k_w = 0.0313$	0.00	0.24	0.25	0.26	0.31	0.34	0.35	0.36	0.37	0.37
$\sigma = 0^\circ$ $k_w = 0.0500$	0.00	0.22	0.23	0.24	0.27	0.28	0.29	0.29	0.29	0.29
$\sigma = 8^\circ$ $k_w = 0.0313$	0.00	0.24	0.28	0.32	0.35	0.37	0.38	0.39	0.39	0.39
$\sigma = 8^\circ$ $k_w = 0.0500$	0.00	0.21	0.24	0.27	0.29	0.30	0.30	0.31	0.31	0.31

3.2 Atmospheric stratification

Atmospheric stratification cases correspond also to the schematics in Fig. 6. As with the sector variation cases, negligible differences from the simulations were found for all stability cases when averaging rows 2–7 compared to take row 7 alone (so the results for the latter case are shown only).

All stability cases are analyzed for the wind direction size $270 \pm 5^\circ$. The simulations were performed with k_w-values evaluated for each stability condition based on Eq. (4). For neutral conditions $\psi_m(h/L) = 0$ and so $k_w = 0.0313$. It is however not straightforward to estimate $\psi_m(h/L)$ for non-neutral conditions as we need a "common" L-value for each condition. The ideal modeling scenario would be to simulate each 10-min case observed using each 10-min L-value. However we don't have the data from which the average for each stability conditions was made. Therefore, we estimate L by using the results from Peña et al. (2013), who also perform and atmospheric stability analysis at Horns Rev I and estimated a correspondent L-value for each stability conditions based on 10-min L estimations. The result is $k_w = 0.0340$ and $k_w = 0.0230$ for unstable and stable conditions, respectively.

3.2.1 Unstable case

Figure 11 and Table 5 show the results for this case with $k_w = 0.0340$ with $\sigma = 0^\circ$ and $\sigma = 8^\circ$. The figure also shows the results of the other two stability cases. We choose to perform simulations with $\sigma = 8^\circ$ assuming that part of the direction uncertainty is due to the large scale meandering behavior of the wakes, which is higher under unstable compared to stable conditions. As expected, the simulations for unstable conditions show the lowest power deficits with and without direction uncertainty as k_w is the highest.

Table 5: Results for the unstable case with wind direction $270 \pm 5^\circ$

distance [m] Model run	0	560	1120	1680	2240	2800	3360	3920	4480	5040
$\sigma = 0^\circ$ $k_w = 0.0340$	0.00	0.54	0.58	0.59	0.60	0.60	0.60	0.60	0.60	0.61
$\sigma = 8^\circ$ $k_w = 0.0340$	0.00	0.33	0.36	0.38	0.40	0.42	0.42	0.43	0.43	0.43

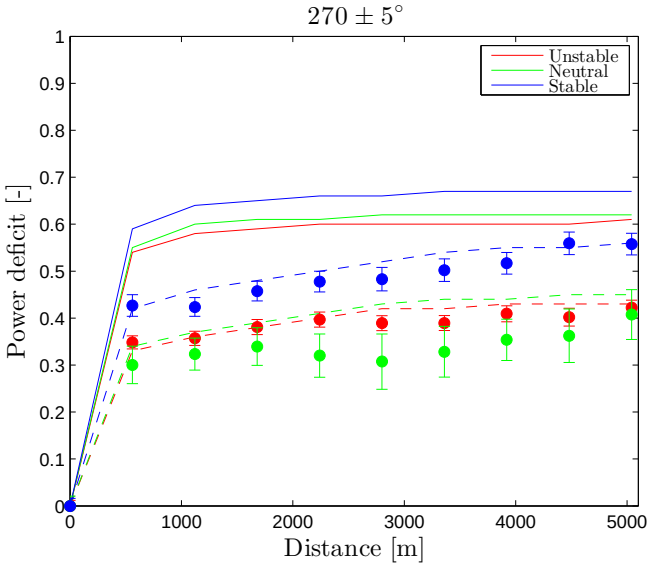

Figure 11: Results for all atmospheric stability cases within the wind direction $270 \pm 5°$. Solid lines correspond to $\sigma = 0°$ and dashed lines to $\sigma = 8°$, $8°$, and $6°$, for unstable, neutral, and stable conditions, respectively. Observations are shown in markers and the error bars provide their uncertainty

3.2.2 Neutral case

The results for the neutral case are also illustrated in Figure 11 and shown in Table 6 with $k_w = 0.0313$ with $\sigma = 0°$ and $\sigma = 8°$, following the flow sector variation cases parameters as we assume that in those cases the conditions are "in average" near neutral. Thus, the simulation results are just between the flow sector variation cases $270 \pm 2.5°$ and $270 \pm 7.5°$.

Table 6: Results for the neutral case with wind direction $270 \pm 5°$

distance [m] Model run	0	560	1120	1680	2240	2800	3360	3920	4480	5040
$\sigma = 0°$ $k_w = 0.0313$	0.00	0.55	0.60	0.61	0.61	0.62	0.62	0.62	0.62	0.62
$\sigma = 8°$ $k_w = 0.0313$	0.00	0.34	0.37	0.39	0.41	0.43	0.44	0.44	0.45	0.45

3.2.3 Stable case

The results for the stable case are also illustrated in Figure 11 and shown in Table 7 with $k_w = 0.0230$ with $\sigma = 0°$ and $\sigma = 6°$. We choose for this particular case to reduce the direction uncertainty as we expect less meandering from the wakes. The simulation results for this case show the highest power deficits as expected, since the k_w value is the lowest.

3.3 Turbulence intensity

3.3.1 Flow sector $250 - 290°$ and 7D spacing

This case takes into account turbines 07 and 17 only, as shown in Fig. 12, and a large variation of directions centered at $270°$. Figure 13 and Table 8 show the results of the simulations with $k_w = 0.0500$ and $k_w = 0.0313$ (so we assume that for each wind direction the conditions are

Table 7: Results for the stable case with wind direction $270 \pm 5^\circ$

distance [m] Model run	0	560	1120	1680	2240	2800	3360	3920	4480	5040
$\sigma = 0^\circ$ $k_w = 0.0230$	0.00	0.59	0.64	0.65	0.66	0.66	0.67	0.67	0.67	0.67
$\sigma = 6^\circ$ $k_w = 0.0230$	0.00	0.42	0.46	0.48	0.50	0.52	0.54	0.55	0.55	0.56

in average near neutral) with $\sigma = 0^\circ$ and $\sigma = 5^\circ$. Although for each direction the direction size is given from the SCADA analysis as 2.5°, we decide to post-processed the simulations with $\sigma = 5^\circ$ (lower than the previous cases), as the results of the SCADA analysis in the range $[250 : 1 : 290]^\circ$ are processed using a 5° moving average window, thus reducing the wind direction uncertainty.

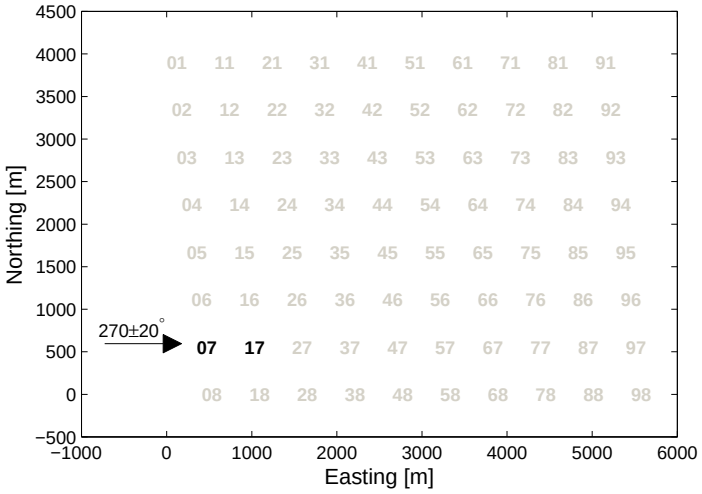

Figure 12: Schematics of the turbines analyzed for the turbulence intensity case with 7D spacing

As expected, the simulations using lower k_w values show higher power deficits around 270°. However, for both types of post-processing (with and without direction uncertainty), $k_w = 0.0500$-results show higher power deficits. For the $\sigma = 0^\circ$ cases, this occurs at $\sim 270 \pm 6^\circ$ as the broader wake from turbine 07 simulated using $k_w = 0.0500$ will be hitting a larger area of turbine 17 compared to that using $k_w = 0.0313$. No wake is seen by turbine 17 at directions outside the range $\sim 270 \pm 12^\circ$.

When post-processing using the direction uncertainty, we keep on accounting for wakes coming from directions close to 270°, although the "analyzed" direction is closer to the limits of the interval. Therefore, these simulations show higher power deficits than those with $\sigma = 0^\circ$ at $\sim 270 \pm 6^\circ$.

3.3.2 Flow sector $90 \pm 2.5^\circ$ and 7D spacing

This case takes into account turbines 95 and 85 only, as shown in Fig. 14, and a narrow direction size of $\pm 2.5^\circ$. Figure 15 and Table 9 show the results of the simulations with $\sigma = 0^\circ$ and $\sigma = 6^\circ$. k_w is estimated from Eq. (5) for the different values of TI in Table 9.

As with the previous 270° cases, simulations post-processed without taking into account

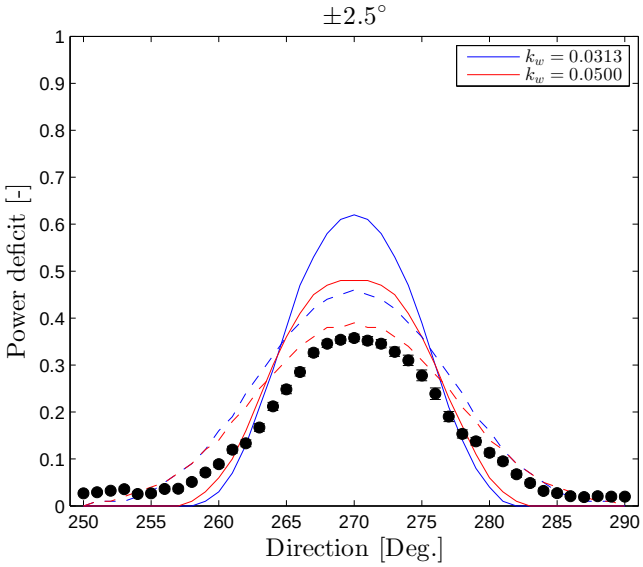

Figure 13: Results for the flow sector $250 - 290°$ and 7D spacing case. Solid and dashed lines correspond to $\sigma = 0°$ and $\sigma = 5°$, respectively. Observations are shown in markers and the error bars provide their uncertainty

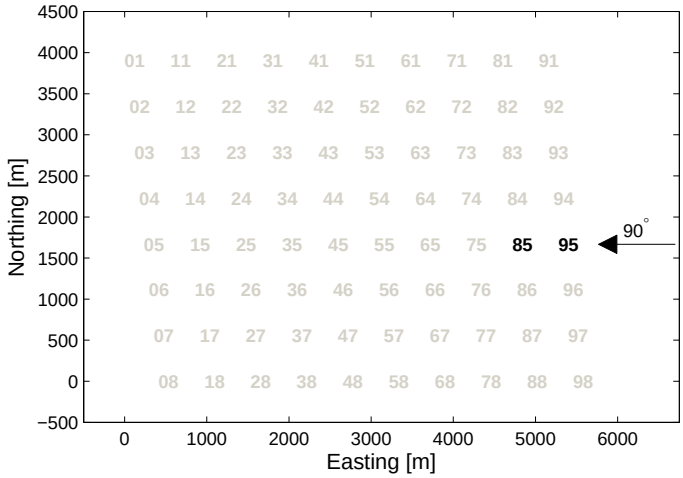

Figure 14: Schematics of the turbines analyzed for the turbulence intensity case with 7D spacing

the direction uncertainty show much larger power deficits. The power deficits are lower when increasing TI as this results in increasing k_w-values. The slope of the lines made by the results decreases in magnitude as we account for uncertainty as we partly account for the wake directly upstream turbine 85, although the direction might be, e.g. $\neq 90°$.

3.3.3 Flow sector $132 \pm 2.5°$ and 10.4D spacing

This case takes into account turbines 95 and 84 only, as shown in Fig. 16, and a narrow direction size of $\pm 2.5°$. Figure 17 and Table 10 show the results of the simulations with $\sigma = 0°$ and $\sigma = 6°$. k_w is also estimated from Eq. (5) for the different values of TI in Table 10.

Table 8: Results for the flow sector $250 - 290^\circ$ and 7D spacing case

Direction [Deg.]	Model run			
	$\sigma = 0^\circ$ $k_w = 0.0313$	$\sigma = 0^\circ$ $k_w = 0.0500$	$\sigma = 5^\circ$ $k_w = 0.0313$	$\sigma = 5^\circ$ $k_w = 0.0500$
250	0.00	0.00	0.00	0.00
251	0.00	0.00	0.01	0.01
252	0.00	0.00	0.01	0.01
253	0.00	0.00	0.01	0.02
254	0.00	0.00	0.02	0.03
255	0.00	0.00	0.03	0.04
256	0.00	0.00	0.05	0.05
257	0.00	0.00	0.07	0.07
258	0.00	0.01	0.09	0.09
259	0.01	0.03	0.12	0.12
260	0.03	0.06	0.16	0.14
261	0.07	0.10	0.19	0.18
262	0.13	0.16	0.24	0.21
263	0.21	0.23	0.28	0.25
264	0.29	0.30	0.32	0.28
265	0.38	0.36	0.36	0.31
266	0.47	0.41	0.39	0.34
267	0.53	0.45	0.42	0.36
268	0.58	0.47	0.44	0.38
269	0.61	0.48	0.45	0.38
270	0.62	0.48	0.46	0.39
271	0.61	0.48	0.45	0.38
272	0.58	0.47	0.44	0.38
273	0.53	0.45	0.42	0.36
274	0.47	0.41	0.39	0.34
275	0.39	0.36	0.36	0.31
276	0.30	0.30	0.32	0.28
277	0.21	0.23	0.28	0.25
278	0.14	0.17	0.24	0.21
279	0.08	0.11	0.19	0.18
280	0.04	0.06	0.16	0.14
281	0.01	0.03	0.12	0.12
282	0.00	0.01	0.09	0.09
283	0.00	0.00	0.07	0.07
284	0.00	0.00	0.05	0.05
285	0.00	0.00	0.03	0.04
286	0.00	0.00	0.02	0.03
287	0.00	0.00	0.01	0.02
288	0.00	0.00	0.01	0.01
289	0.00	0.00	0.01	0.01
290	0.00	0.00	0.00	0.00

A similar behavior of the simulation results are observed for the range of TI values as the 7D spacing case, except that with this larger spacing, the power deficits considerably decrease as expected (for the simulation using $\sigma = 0^\circ$ the deficit at TI $= 12\%$ is 0.37, whereas it is 0.5 for the 7D spacing case).

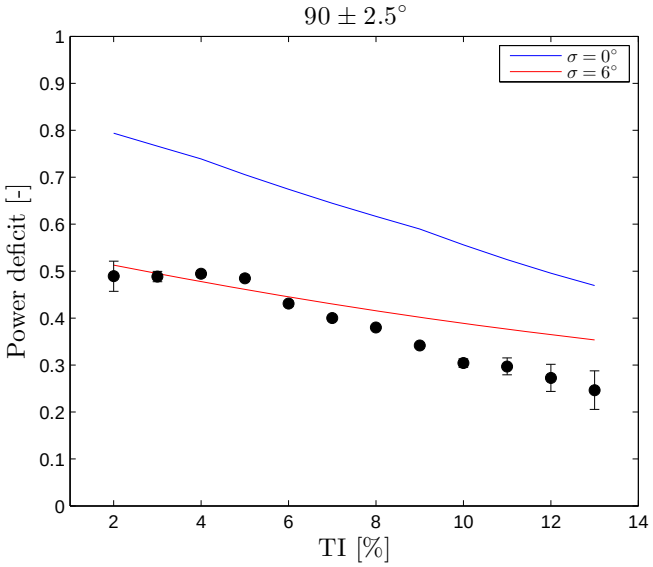

Figure 15: Results for the flow sector $90 \pm 2.5^\circ$ and 7D spacing case. Observations are shown in markers and the error bars provide their uncertainty

Table 9: Results for the flow sector $90 \pm 2.5^\circ$ and 7D spacing case

T.I. [%] Model run	2	3	4	5	6	7	8	9	10	11	12	13
$\sigma = 0^\circ$	0.79	0.77	0.74	0.71	0.67	0.64	0.62	0.59	0.56	0.52	0.50	0.47
$\sigma = 6^\circ$	0.51	0.50	0.48	0.46	0.45	0.43	0.42	0.40	0.39	0.38	0.36	0.35

3.4 Spacing

3.4.1 7D spacing and $270 \pm 5^\circ$

This first spacing case is nearly identical as the flow sector variation cases illustrated in Fig. 6, except for the direction size of $\pm 5^\circ$. Figure 18 and Table 11 show the results of the

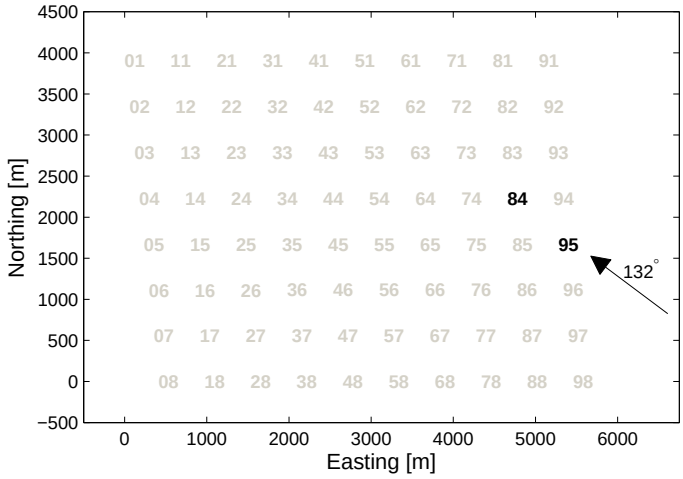

Figure 16: Schematics of the turbines analyzed for the turbulence intensity case with 10.4D spacing

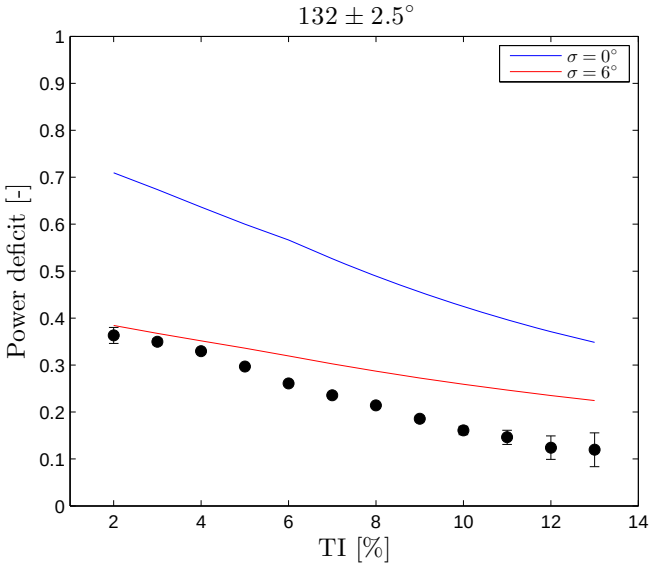

Figure 17: Results for the flow sector $132 \pm 2.5^\circ$ and 10.4D spacing case. Observations are shown in markers and the error bars provide their uncertainty

Table 10: Results for the flow sector $132 \pm 2.5^\circ$ and 10.4D spacing case

T.I. [%]	2	3	4	5	6	7	8	9	10	11	12	13
Model run												
$\sigma = 0^\circ$	0.71	0.67	0.64	0.60	0.57	0.53	0.49	0.46	0.42	0.40	0.37	0.35
$\sigma = 6^\circ$	0.38	0.37	0.35	0.34	0.32	0.30	0.29	0.27	0.26	0.25	0.24	0.22

simulations with $k_w = 0.0500$ and $k_w = 0.0313$ (so we also assume that for each wind direction the conditions are in average near neutral) with $\sigma = 0^\circ$ and $\sigma = 8^\circ$ in consistency with the analysis performed in flow sector variation cases. As expected the simulation results are just between those for the flow sector variation cases $270 \pm 2.5^\circ$ and $270 \pm 7.5^\circ$.

Table 11: Results for the 7D spacing and wind direction $270 \pm 5^\circ$ test case

distance [m]	0	560	1120	1680	2240	2800	3360	3920	4480	5040
Model run										
$\sigma = 0^\circ$ $k_w = 0.0313$	0.00	0.56	0.60	0.61	0.62	0.62	0.62	0.62	0.62	0.63
$\sigma = 0^\circ$ $k_w = 0.0500$	0.00	0.46	0.50	0.51	0.52	0.52	0.52	0.52	0.52	0.52
$\sigma = 8^\circ$ $k_w = 0.0313$	0.00	0.34	0.37	0.39	0.42	0.43	0.44	0.45	0.45	0.45
$\sigma = 8^\circ$ $k_w = 0.0500$	0.00	0.30	0.32	0.34	0.35	0.36	0.36	0.36	0.36	0.36

3.4.2 9.4D spacing and $221 \pm 5^\circ$

This case takes into account the diagonal row of turbines illustrated in Fig. 19, and a direction size of $\pm 5^\circ$. Figure 20 and Table 12 show the results of the simulations with $\sigma = 0^\circ$ and

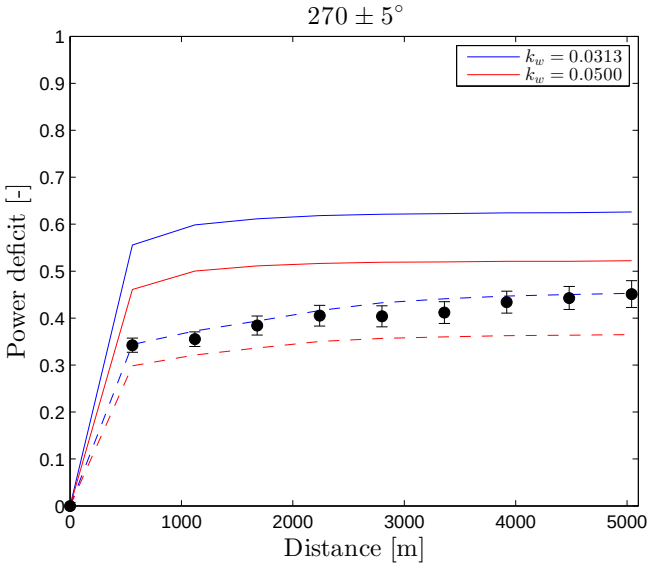

Figure 18: Results for the 7D spacing and wind direction $270 \pm 5^\circ$ test case. Solid and dashed lines correspond to $\sigma = 0^\circ$ and $\sigma = 8^\circ$, respectively. Observations are shown in markers and the error bars provide their uncertainty

$\sigma = 7^\circ$ using two values of k_w (0.0500 and 0.0313; for the latter we assume that the general conditions of the SCADA are near neutral). As expected the simulations show the same behavior as for the 7D case, except that the power deficits are lower as the spacing is larger.

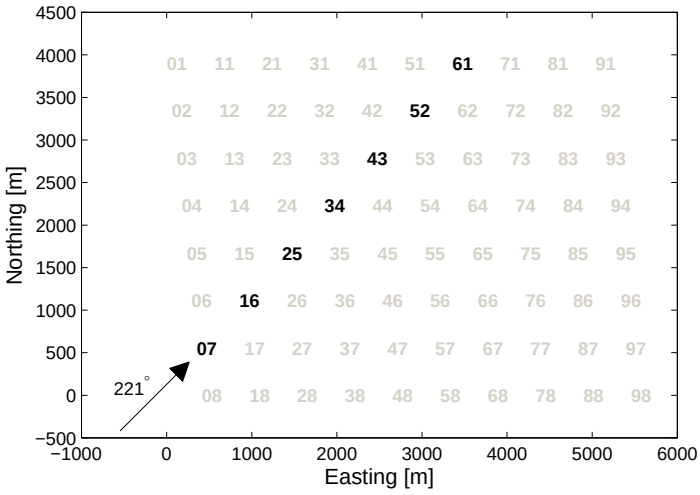

Figure 19: Schematics of the turbines analyzed for the turbulence intensity case with 9.4D spacing

3.4.3 10.4D spacing and $132 \pm 5^\circ$

This case takes into account the diagonal row of turbines illustrated in Fig. 21, and a direction size of $\pm 5^\circ$. Figure 22 and Table 13 show the results of the simulations with $\sigma = 0^\circ$ and $\sigma = 6^\circ$ using two values of k_w (0.0500 and 0.0313; for the latter we assume that the general conditions of the SCADA are near neutral). As expected the simulations show the same

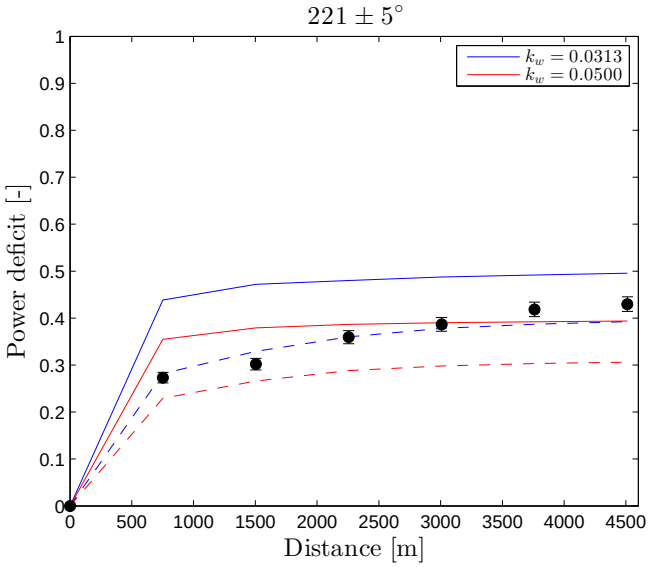

Figure 20: Results for the 9.4D spacing and wind direction $221 \pm 5^\circ$ test case. Solid and dashed lines correspond to $\sigma = 0^\circ$ and $\sigma = 7^\circ$, respectively. Observations are shown in markers and the error bars provide their uncertainty

Table 12: Results for the 9.4D spacing and wind direction $221 \pm 5^\circ$ test case

distance [m] Model run	0	752	1504	2256	3008	3760	4512
$\sigma = 0^\circ$ $k_w = 0.0313$	0.00	0.44	0.47	0.48	0.49	0.49	0.50
$\sigma = 0^\circ$ $k_w = 0.0500$	0.00	0.35	0.38	0.39	0.39	0.39	0.39
$\sigma = 7^\circ$ $k_w = 0.0313$	0.00	0.28	0.33	0.36	0.38	0.39	0.39
$\sigma = 7^\circ$ $k_w = 0.0500$	0.00	0.23	0.27	0.29	0.30	0.30	0.31

behavior as for the 7D and 9.4D cases, except that the power deficits are here lower as the spacing is also larger.

Table 13: Results for the 10.4D spacing and wind direction $132 \pm 5^\circ$ test case

distance [m] Model run	0	832	1664	2496	3328	4160	4992
$\sigma = 0^\circ$ $k_w = 0.0313$	0.00	0.41	0.44	0.45	0.45	0.46	0.46
$\sigma = 0^\circ$ $k_w = 0.0500$	0.00	0.33	0.35	0.35	0.36	0.36	0.36
$\sigma = 6^\circ$ $k_w = 0.0313$	0.00	0.28	0.33	0.36	0.37	0.38	0.39
$\sigma = 6^\circ$ $k_w = 0.0500$	0.00	0.22	0.26	0.28	0.29	0.29	0.29

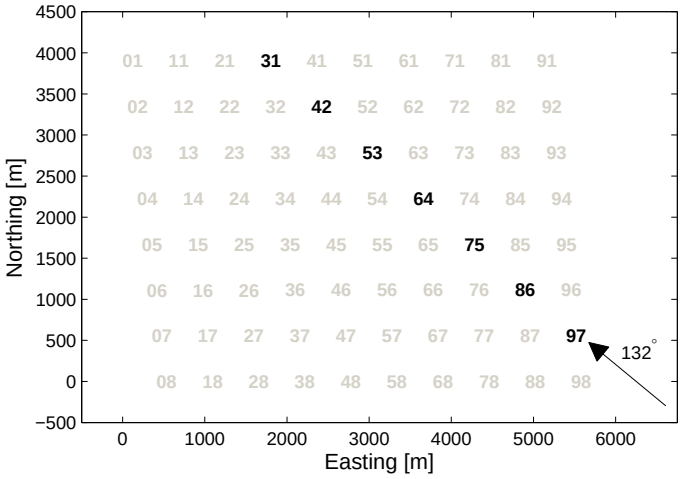

Figure 21: Schematics of the turbines analyzed for the turbulence intensity case with 10.4D spacing

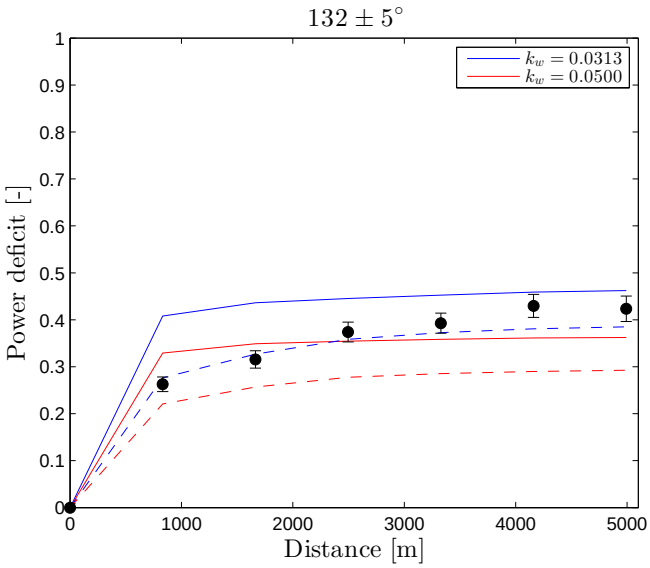

Figure 22: Results for the 10.4D spacing and wind direction $132 \pm 5°$ test case. Solid and dashed lines correspond to $\sigma = 0°$ and $\sigma = 6°$, respectively. Observations are shown in markers and the error bars provide their uncertainty

3.5 Park efficiency

For the park efficiency, estimated using Eq. (7), we perform simulations within the interval $[0 : 0.1 : 360]°$ with $k_w = 0.0500$ and $k_w = 0.0313$ (so we assume near neutral atmospheric conditions for all wind directions). The post-processing is performed using $\sigma = 0°$ and $\sigma = 4°$. We have a relative low value for the wind direction uncertainty as the results of the analysis of the SCADA data had probably been subjected to some sort of moving averaging, which reduces some of the uncertainty. The results are shown in a polar form in Fig. 23 and in Table 14.

All simulations show the lowest efficiencies caused by wakes at the wind directions $90°$ and $270°$ as for these two cases there is a large number of wake-affected wind turbines. There are also two cases close to $0°$ and $180°$ (offset $5°$ counterclockwise as the wind farm

Table 14: The park efficiency of the Horns Rev I wind farm as a function of wind direction

Model run Direction [Deg.]	$\sigma = 0^\circ$ $k_w = 0.0313$	$\sigma = 0^\circ$ $k_w = 0.0500$	$\sigma = 4^\circ$ $k_w = 0.0313$	$\sigma = 4^\circ$ $k_w = 0.0500$
0	0.73	0.73	0.68	0.72
5	0.92	0.94	0.85	0.87
10	0.87	0.91	0.87	0.91
15	0.87	0.90	0.84	0.89
20	0.77	0.83	0.80	0.86
25	0.82	0.86	0.82	0.87
30	0.88	0.93	0.86	0.89
35	0.88	0.88	0.79	0.83
40	0.59	0.68	0.67	0.74
45	0.65	0.71	0.69	0.75
50	0.90	0.91	0.82	0.85
55	0.87	0.92	0.85	0.89
60	0.78	0.83	0.80	0.86
65	0.79	0.84	0.79	0.85
70	0.84	0.90	0.83	0.88
75	0.86	0.91	0.86	0.90
80	0.90	0.91	0.81	0.84
85	0.64	0.66	0.61	0.67
90	0.37	0.51	0.49	0.59
95	0.63	0.65	0.61	0.67
100	0.89	0.91	0.80	0.84
105	0.86	0.91	0.85	0.90
110	0.84	0.88	0.82	0.88
115	0.74	0.84	0.80	0.86
120	0.85	0.89	0.82	0.87
125	0.88	0.89	0.80	0.84
130	0.63	0.71	0.70	0.76
135	0.68	0.74	0.71	0.78
140	0.89	0.92	0.82	0.86
145	0.83	0.88	0.82	0.88
150	0.77	0.85	0.81	0.87
155	0.86	0.90	0.84	0.89
160	0.88	0.92	0.87	0.90
165	0.89	0.89	0.79	0.82
170	0.56	0.61	0.59	0.65
175	0.41	0.53	0.51	0.61
180	0.73	0.73	0.68	0.72
185	0.92	0.94	0.85	0.87
190	0.87	0.91	0.87	0.91
195	0.87	0.90	0.84	0.89
200	0.77	0.83	0.80	0.86
205	0.82	0.86	0.82	0.87
210	0.88	0.93	0.86	0.89
215	0.88	0.88	0.79	0.83
220	0.59	0.68	0.67	0.74
225	0.65	0.71	0.69	0.75
230	0.90	0.91	0.82	0.85
235	0.87	0.92	0.85	0.89
240	0.78	0.83	0.80	0.86
245	0.79	0.84	0.79	0.85
250	0.84	0.90	0.83	0.88
255	0.86	0.91	0.86	0.90
260	0.90	0.91	0.81	0.84
265	0.64	0.66	0.61	0.67
270	0.37	0.51	0.49	0.59
275	0.63	0.65	0.61	0.67
280	0.89	0.91	0.80	0.84
285	0.86	0.91	0.85	0.90
290	0.84	0.88	0.82	0.88
295	0.74	0.84	0.80	0.86
300	0.85	0.89	0.82	0.87
305	0.88	0.89	0.80	0.84
310	0.63	0.71	0.70	0.76
315	0.68	0.74	0.71	0.78
320	0.89	0.92	0.82	0.86
325	0.83	0.88	0.82	0.88
330	0.77	0.85	0.81	0.87
335	0.86	0.90	0.84	0.89
340	0.88	0.92	0.87	0.90
345	0.89	0.89	0.79	0.82
350	0.56	0.61	0.59	0.65
355	0.41	0.53	0.51	0.61

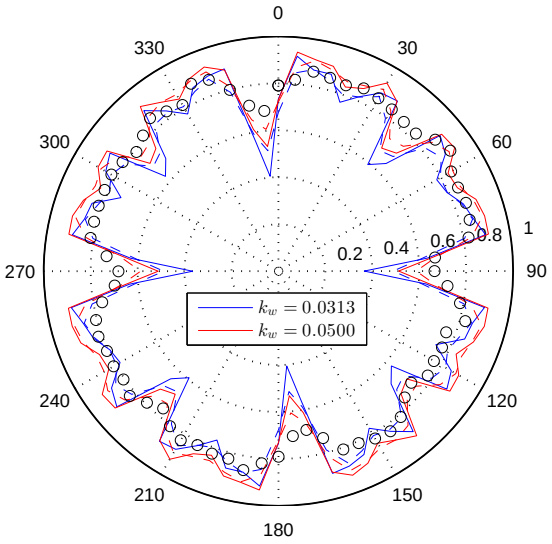

Figure 23: The park efficiency of the Horns Rev I wind farm. Solid and dashed lines correspond to $\sigma = 0°$ and $\sigma = 4°$, respectively. Observations are shown in markers

is slightly oblique), which also show very low efficiencies. It is interesting to see that for these highly wake-affected sectors the results using the direction uncertainty show higher efficiencies (compared to the $\sigma = 0°$ cases), whereas for those sectors with general higher efficiencies, e.g. that between $240°$ and $260°$, both cases (with and without uncertainty) show similar efficiencies as the uncertainty ones just slightly account for directions where the wake is highest.

4 Lillgrund cases

The simulations are, unless otherwise stated, performed with two k_w-values: 0.0500 (WAsP recommended) and $k_w = 0.0313$ assuming $u_{hfree} = 9$ m s^{-1}. The latter results by evaluating Eq. (4) with the Siemens turbine specifications in Section 2.2 using $z_o = 0.0002$ m and $\psi_m(h/L) = 0$ as in the Horns Rev I cases. Further, results using $\sigma = 0°$ and $\sigma = 4°$ are also computed. We choose this direction uncertainty value as we do not have more information about the variability of the wind at Lillgrund. Also, this value is chosen to be slightly lower than that used for the Horns Rev I cases as Lillgrund is located in the Baltic Sea, where more stable conditions are observed compared to the North Sea. Observations and data treatment are described in Hansen (2013b).

4.1 Sector variation

4.1.1 3.3D spacing $120°$

This case takes into account the row of turbines shown in Fig. 24 and a variation of directions centered at $120°$ with a size each of $\pm 2.5°$. Figure 25 and Tables 15 and 16 show the results of the simulations.

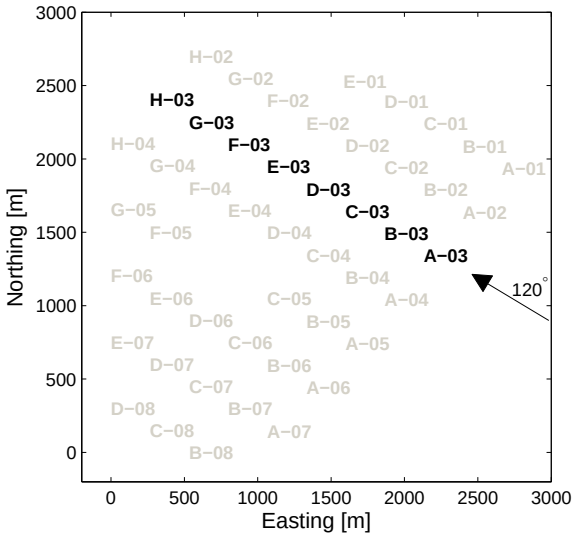

Figure 24: Schematics of the turbines analyzed for the sector variation case with 3.3D spacing

For the wind directions not parallel to $120°$, the results using the wind direction uncertainty show slightly higher power deficits than those without it as, by using the uncertainty, we account for those directions where the deficit is the highest. At $120°$ the power deficits are the highest, as this direction is parallel to the row and they are lower as the wind turns to either side. At $\pm 20°$ and further, the power deficits simulated at the second turbine (B-03) up to the fourth (D-03) (for the $\sigma = 0°$ case) are nearly constant as the other turbines on the rows parallel to this do not shade those turbines. This effect is not so noticeable for the $\sigma = 4°$ case as the wakes from turbines are still accounted for.

4.1.2 4.3D spacing $222°$

This case takes into account the row of turbines shown in Fig. 26 and a variation of directions centered at $222°$ with a size each of $\pm 2.5°$. Figure 27 and Tables 17 and 18 show the results of the simulations.

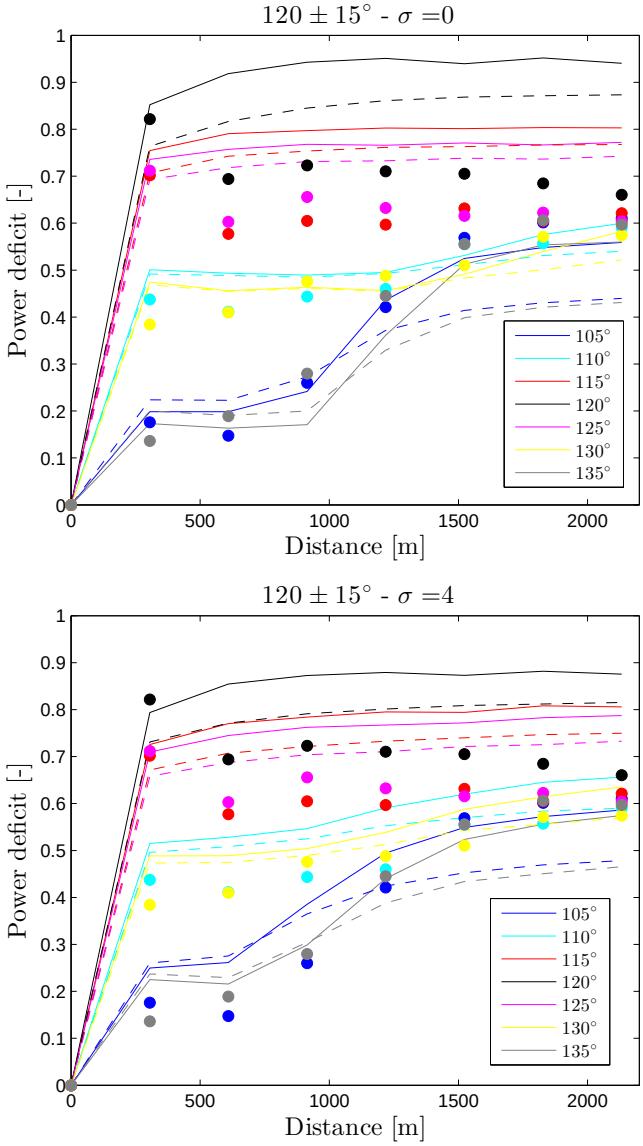

Figure 25: Results for the 3.3D spacing $120°$ sector variation case. Solid and dashed lines correspond to $k_w = 0.0313$ and $k_w = 0.0500$, respectively, without (top frame) and with (bottom frame) direction uncertainty. Observations are shown in markers

Table 15: Results for the 3.3D spacing $120°$ sector variation case with $k_w = 0.0313$ and $\sigma = 0°$

Direction [Deg.] / Distance [m]	105	110	115	120	125	130	135
0	0	0	0	0	0	0	0
305	0.20	0.50	0.75	0.85	0.74	0.47	0.17
609	0.20	0.49	0.79	0.92	0.76	0.46	0.16
914	0.24	0.49	0.80	0.94	0.77	0.46	0.17
1218	0.44	0.50	0.80	0.95	0.77	0.46	0.36
1523	0.52	0.53	0.80	0.94	0.77	0.49	0.51
1828	0.55	0.58	0.80	0.95	0.77	0.54	0.55
2132	0.56	0.60	0.80	0.94	0.77	0.58	0.56

Table 16: Results for the 3.3D spacing 120° sector variation case with $k_w = 0.0313$ and $\sigma = 4^\circ$

Direction [Deg.] Distance [m]	105	110	115	120	125	130	135
0	0	0	0	0	0	0	0
305	0.25	0.52	0.73	0.79	0.71	0.49	0.23
609	0.26	0.53	0.77	0.85	0.74	0.49	0.22
914	0.39	0.55	0.78	0.87	0.76	0.50	0.30
1218	0.49	0.59	0.80	0.88	0.77	0.54	0.44
1523	0.55	0.62	0.79	0.87	0.77	0.59	0.52
1828	0.57	0.65	0.81	0.88	0.78	0.61	0.56
2132	0.59	0.66	0.81	0.88	0.79	0.64	0.57

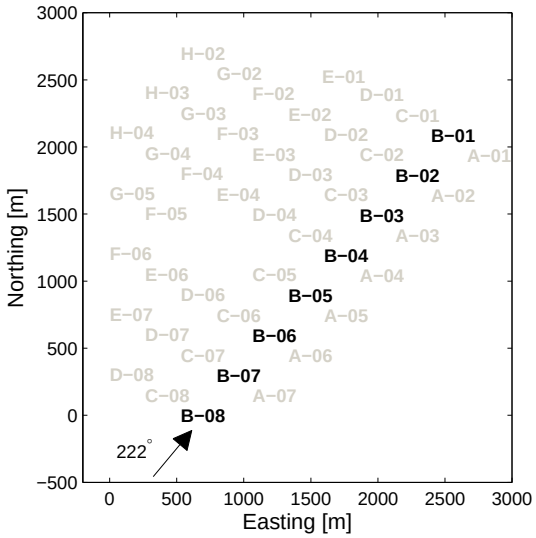

Figure 26: Schematics of the turbines analyzed for the sector variation case with 4.3D spacing

Table 17: Results for the 4.3D spacing 222° sector variation case with $k_w = 0.0313$ and $\sigma = 0^\circ$

Direction [Deg.] Distance [m]	207	212	217	222	227	232	237
0	0	0	0	0	0	0	0
391	0.03	0.32	0.66	0.80	0.65	0.30	0.03
794	0.04	0.32	0.69	0.87	0.65	0.28	0.37
1191	0.14	0.31	0.69	0.89	0.67	0.44	0.54
1588	0.51	0.40	0.69	0.90	0.67	0.54	0.56
1984	0.54	0.51	0.70	0.90	0.69	0.56	0.59
2381	0.54	0.56	0.71	0.91	0.70	0.58	0.61
2778	0.54	0.57	0.72	0.91	0.71	0.59	0.60

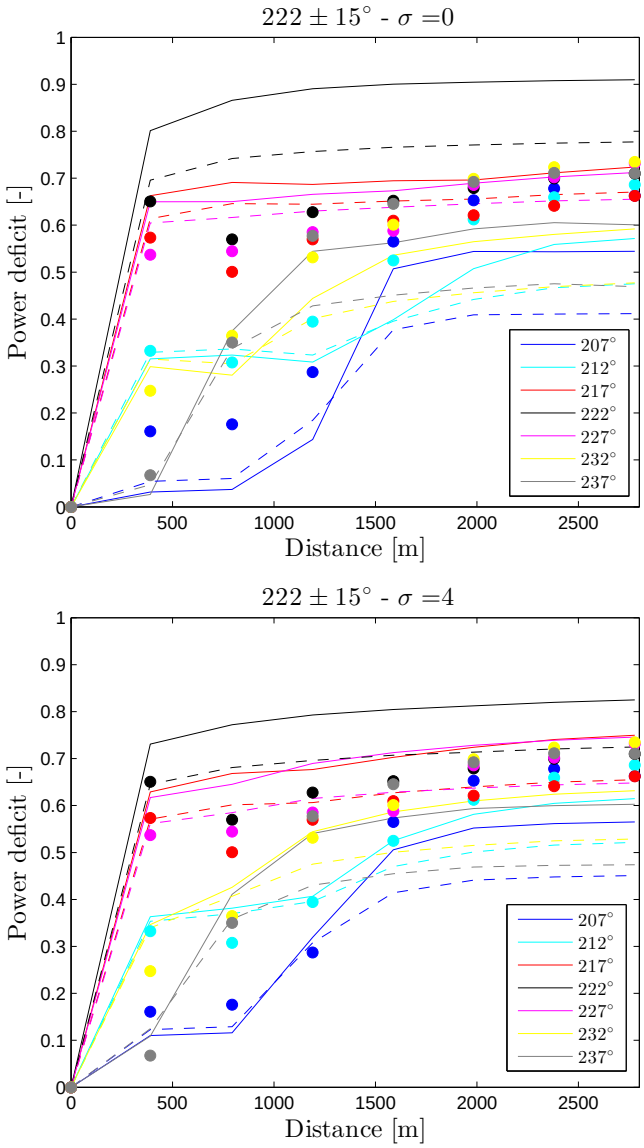

Figure 27: Results for the 4.3D spacing 222° sector variation case. Solid and dashed lines correspond to $k_w = 0.0313$ and $k_w = 0.0500$, respectively, without (top frame) and with (bottom frame) direction uncertainty. Observations are shown in markers

Table 18: Results for the 4.3D spacing 222° sector variation case with $k_w = 0.0313$ and $\sigma = 4°$

Direction [Deg.] / Distance [m]	207	212	217	222	227	232	237
0	0	0	0	0	0	0	0
391	0.11	0.36	0.63	0.73	0.62	0.35	0.11
794	0.12	0.38	0.67	0.77	0.65	0.43	0.41
1191	0.32	0.41	0.68	0.79	0.69	0.54	0.54
1588	0.51	0.53	0.70	0.80	0.71	0.59	0.57
1984	0.55	0.58	0.72	0.81	0.73	0.61	0.59
2381	0.56	0.60	0.74	0.82	0.74	0.62	0.60
2778	0.57	0.61	0.75	0.83	0.75	0.63	0.60

Similar to the previous case, the results using the wind direction uncertainty show slightly higher power deficits (for those wind directions not parallel to the row). At 222° the power deficits are the highest, as this direction is the parallel one to the row and they are lower as the wind turns to either side. In this case the simulations show very low power deficits at the first two to three turbines (when the wind directions are offset $\pm 15^\circ$ from 222°) as it is only partial wakes affecting those.

4.2 Speed recovery

4.2.1 3.3D spacing 120° – 2 missing turbines

This case takes into account the row of turbines shown in Fig. 28 with 2 turbines missing and a variation of directions centered at 120° with a size each of $\pm 2.5^\circ$. Figure 29 and Tables 19 and 20 show the results of the simulations.

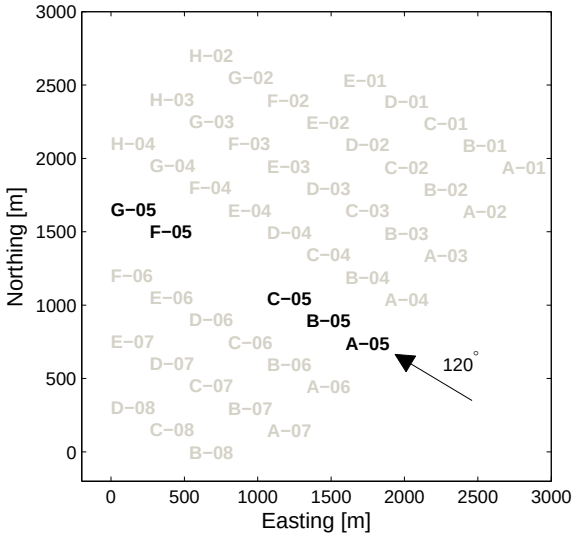

Figure 28: Schematics of the turbines analyzed for the speed deficit case with 3.3D spacing and 2 missing turbines

Table 19: Results for the 3.3D spacing 120° sector variation case with 2 missing turbines and $k_w = 0.0313$ and $\sigma = 0^\circ$

Direction [Deg.] Distance [m]	105	110	115	120	125	130	135
0	0	0	0	0	0	0	0
305	0.20	0.50	0.75	0.85	0.74	0.47	0.17
609	0.20	0.49	0.79	0.92	0.76	0.46	0.16
1523	0.49	0.15	0.31	0.70	0.25	0.11	0.48
1828	0.55	0.58	0.76	0.89	0.74	0.55	0.56

Generally, the simulations show higher power deficits for the results accounting for the direction uncertainty compared to those which do not (when the direction is not parallel to the row). However, after the two missing turbines those without uncertainty show higher deficits, precisely because there are no close upstream wind turbines. Also interesting is that at the furthest wind directions from that parallel to the row (120°), the missing turbines are

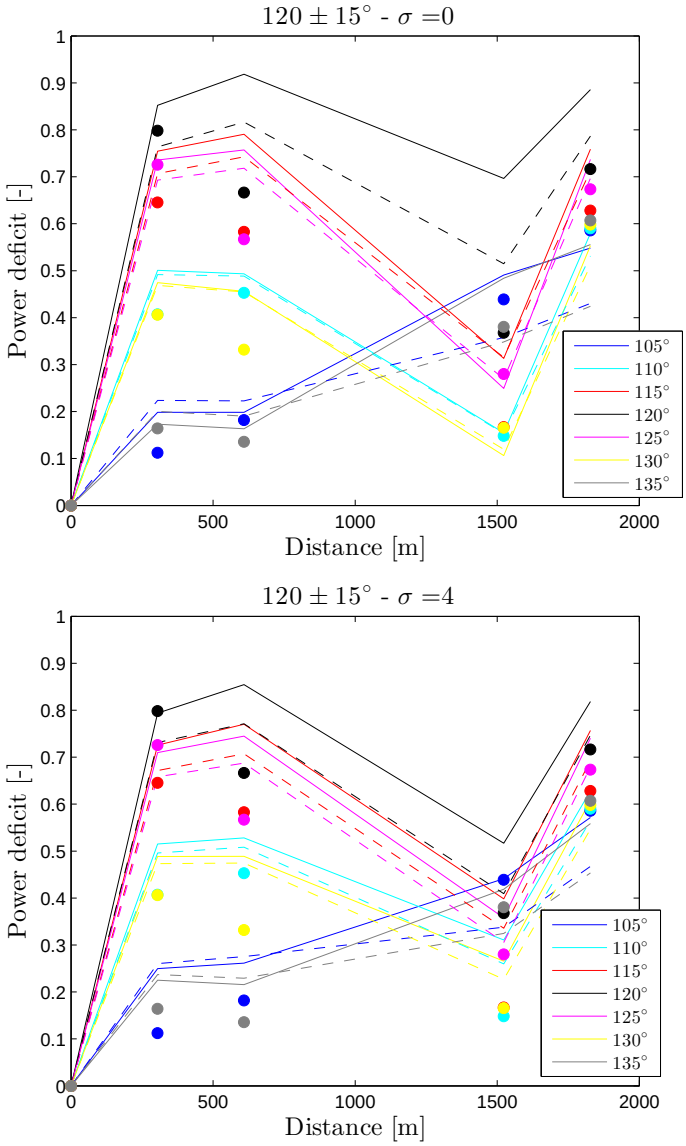

Figure 29: Results for the 3.3D spacing $120°$ speed recovery case with 2 missing turbines. Solid and dashed lines correspond to $k_w = 0.0313$ and $k_w = 0.0500$, respectively, without (top frame) and with (bottom frame) direction uncertainty. Observations are shown in markers

Table 20: Results for the 3.3D spacing $120°$ sector variation case with 2 missing turbines and $k_w = 0.0313$ and $\sigma = 4°$

Direction [Deg.] Distance [m]	105	110	115	120	125	130	135
0	0	0	0	0	0	0	0
305	0.25	0.52	0.73	0.79	0.71	0.49	0.23
609	0.26	0.53	0.77	0.85	0.74	0.49	0.22
1523	0.44	0.31	0.40	0.52	0.36	0.27	0.42
1828	0.57	0.63	0.76	0.82	0.74	0.61	0.56

not clearly observed as the sideways wakes from the turbines parallel to that row also shade turbines F-05 and G-05 and the power deficits at these turbines is anyway higher than those upstream on the same row.

4.2.2 4.3D spacing 222° – 1 missing turbine

This case takes into account the row of turbines shown in Fig. 30 with 1 turbine missing and a variation of directions centered at 222° with a size each of $\pm 2.5^\circ$. Figure 31 and Tables 21 and 22 show the results of the simulations.

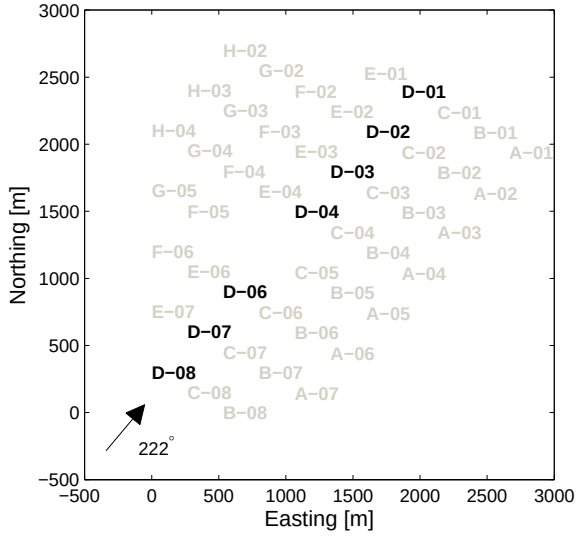

Figure 30: Schematics of the turbines analyzed for the speed deficit case with 4.3D spacing and 1 missing turbine

Table 21: Results for the 4.3D spacing 222° sector variation case with 1 missing turbine and $k_w = 0.0313$ and $\sigma = 0^\circ$

Direction [Deg.] / Distance [m]	207	212	217	222	227	232	237
0	0	0	0	0	0	0	0
397	0.04	0.32	0.67	0.80	0.64	0.29	0.02
794	0.14	0.32	0.69	0.87	0.65	0.28	0.02
1588	0.54	0.39	0.37	0.73	0.32	0.29	0.54
1984	0.57	0.56	0.69	0.85	0.66	0.54	0.39
2381	0.59	0.57	0.72	0.89	0.69	0.48	0.42
2778	0.60	0.58	0.72	0.90	0.70	0.50	0.58

Similarly as for the previous cases, the simulations without direction uncertainty show higher power deficits for wind directions nearly parallel to the row (in this case 222°. The effect of the missing turbine is clearly seen at nearly all directions except those furthest from that parallel to the row. In this case it is also interesting to see the effect of the missing turbine on the row E of turbines on row D (from turbine D-04 downstream).

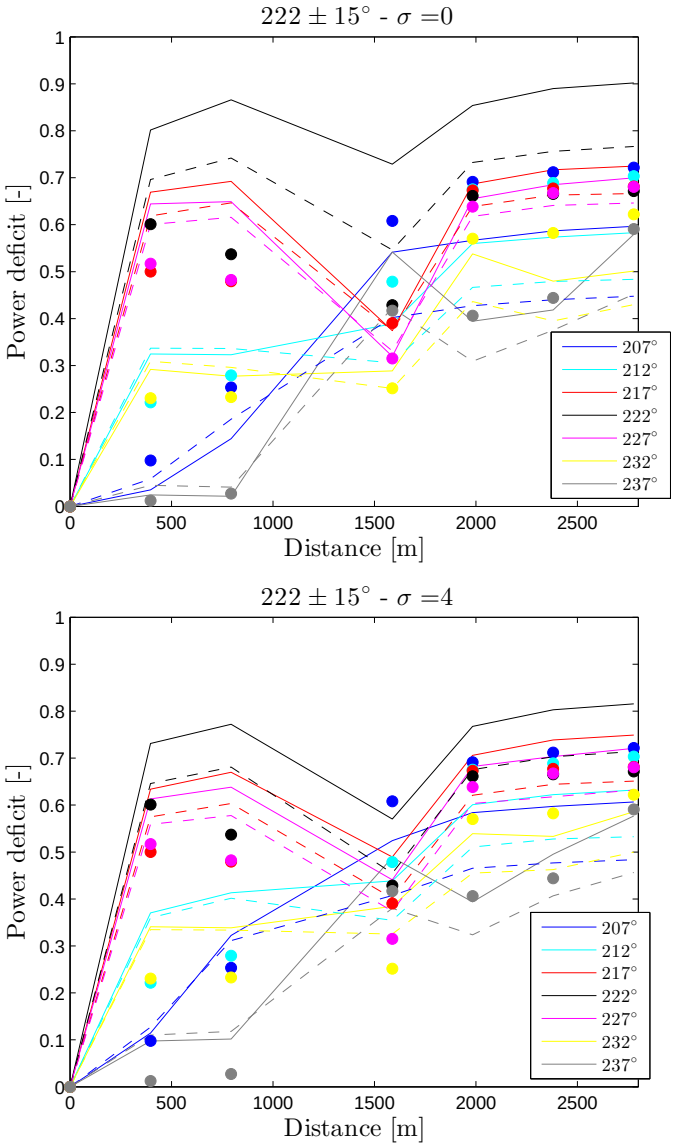

Figure 31: Results for the 4.3D spacing 222° speed recovery case with 1 missing turbine. Solid and dashed lines correspond to $k_w = 0.0313$ and $k_w = 0.0500$, respectively, without (top frame) and with (bottom frame) direction uncertainty. Observations are shown in markers

Table 22: Results for the 4.3D spacing 222° sector variation case with 1 missing turbine and $k_w = 0.0313$ and $\sigma = 4°$

Direction [Deg.] Distance [m]	207	212	217	222	227	232	237
0	0	0	0	0	0	0	0
397	0.11	0.37	0.63	0.73	0.61	0.34	0.10
794	0.32	0.41	0.67	0.77	0.64	0.34	0.10
1588	0.52	0.44	0.49	0.57	0.44	0.38	0.49
1984	0.58	0.60	0.71	0.77	0.68	0.54	0.39
2381	0.60	0.62	0.74	0.80	0.70	0.53	0.50
2778	0.61	0.63	0.75	0.82	0.72	0.59	0.58

4.3 Turbulence intensity

4.3.1 Flow sector $120 \pm 2.5°$ and 3.3D spacing

This case takes into account turbines C-08 and B-08 only, as shown in Fig. 32, and a narrow direction size of $\pm 2.5°$ centered at $270°$ where the spacing is 3.3D. Figure 33 and Table 23 show the results of the simulations with $\sigma = 0°$ and $\sigma = 4°$. k_w is estimated from Eq. (5) for the different values of TI in Table 23.

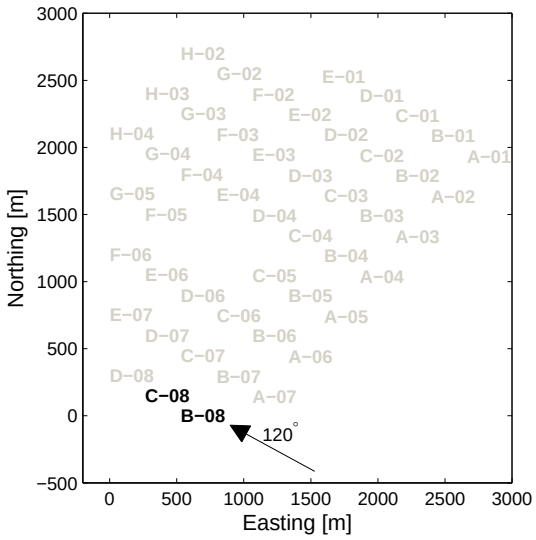

Figure 32: Schematics of the turbines analyzed for the turbulence intensity case with 3.3D spacing

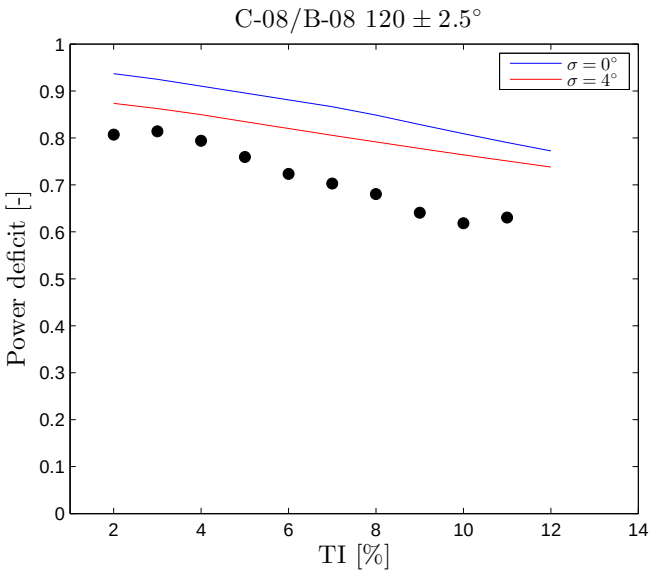

Figure 33: Results for the flow sector $120 \pm 2.5°$ and 3.3D spacing case. Observations are shown in markers

For the Lillgrund cases the power deficits are much higher compared to those at Horns Rev I due to the short distance between turbines. Simulations post-processed without taking into account the direction uncertainty show larger power deficits. The power deficits are lower when increasing TI as this results in increasing k_w-values. The slope of the lines made by the

results decreases in magnitude as we account for uncertainty as we partly account for the wake directly upstream turbine C-08, although the direction might be, e.g. $\neq 120^\circ$

Table 23: Results for the flow sector $120 \pm 2.5^\circ$ and 3.3D spacing case

T.I. [%] Model run	2	3	4	5	6	7	8	9	10	11	12
$\sigma = 0^\circ$	0.94	0.92	0.91	0.90	0.88	0.87	0.85	0.83	0.81	0.79	0.77
$\sigma = 4^\circ$	0.87	0.86	0.85	0.83	0.82	0.81	0.79	0.78	0.76	0.75	0.74

4.3.2 Flow sector $222 \pm 2.5^\circ$ and 4.3D spacing

This case takes into account turbines B-08 and B-07 only, as shown in Fig. 34, and a narrow direction size of $\pm 2.5^\circ$. Figure 35 and Table 24 show the results of the simulations with $\sigma = 0^\circ$ and $\sigma = 4^\circ$. k_w is also estimated from Eq. (5) for the different values of TI in Table 24.

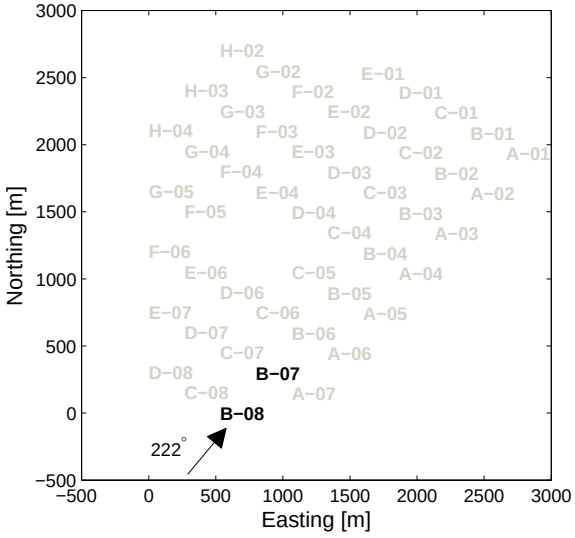

Figure 34: Schematics of the turbines analyzed for the turbulence case with 4.3D spacing

A similar behavior of the simulation results are observed for the range of TI values as the 3.3D spacing case, except that with this larger spacing, the power deficits slightly decrease as expected.

Table 24: Results for the flow sector $222 \pm 2.5^\circ$ and 3.3D spacing case

T.I. [%] Model run	2	3	4	5	6	7	8	9	10	11	12
$\sigma = 0^\circ$	0.92	0.90	0.88	0.86	0.84	0.82	0.80	0.78	0.75	0.73	0.71
$\sigma = 4^\circ$	0.82	0.81	0.79	0.78	0.76	0.74	0.73	0.71	0.69	0.67	0.65

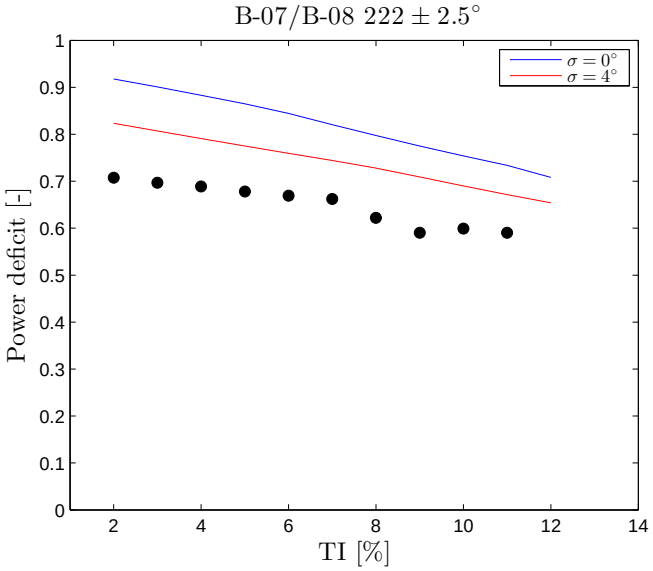

Figure 35: Results for the flow sector $222 \pm 2.5^\circ$ and 3.3D spacing case. Observations are shown in markers

4.4 Park efficiency

For the park efficiency, estimated using Eq. (7), we also perform simulations within the interval $[0 : 0.1 : 360]^\circ$ with $k_w = 0.0500$ and $k_w = 0.0313$ (so we assume near neutral atmospheric conditions for all wind directions). The post-processing is also performed using $\sigma = 0^\circ$ and $\sigma = 4^\circ$, so we assume that the direction uncertainty is the same for all sectors, which might be very different from reality as Lillgrund is located close to the land and for some sectors the direction variability might largely change. The results are shown in a polar form in Fig. 36 and in Table 25.

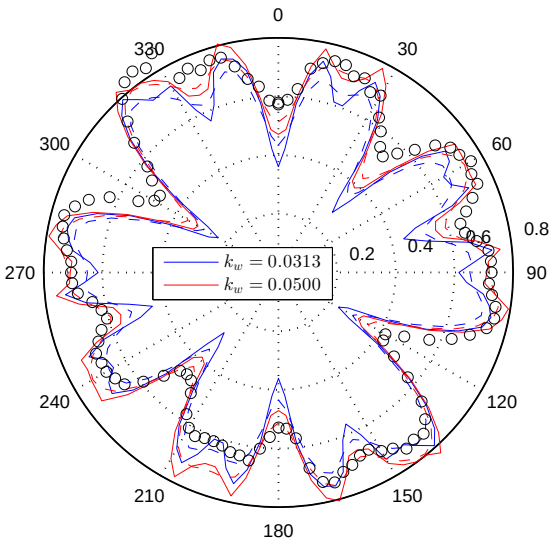

Figure 36: The park efficiency of the Lillgrund wind farm. Solid and dashed lines correspond to $\sigma = 0^\circ$ and $\sigma = 4^\circ$, respectively. Observations are shown in markers

All simulations show the lowest efficiencies caused by wakes at the wind directions 120° and 300° (followed by those at 42° and 222°) as for these two first cases there is a large number of wake-affected rows of wind turbines and very closed spaced. There are also two cases (0° and

Table 25: The park efficiency of the Lillgrund wind farm as a function of wind direction

Model run	$\sigma = 0^\circ$	$\sigma = 0^\circ$	$\sigma = 4^\circ$	$\sigma = 4^\circ$	Model run	$\sigma = 0^\circ$	$\sigma = 0^\circ$	$\sigma = 4^\circ$	$\sigma = 4^\circ$
	$k_w =$	$k_w =$	$k_w =$	$k_w =$		$k_w =$	$k_w =$	$k_w =$	$k_w =$
Direction [Deg.]	0.0313	0.0500	0.0313	0.0500	Direction [Deg.]	0.0313	0.0500	0.0313	0.0500
0	0.36	0.47	0.43	0.51	183	0.42	0.49	0.46	0.54
3	0.42	0.49	0.46	0.54	186	0.58	0.60	0.54	0.59
6	0.58	0.60	0.54	0.59	189	0.68	0.71	0.62	0.67
9	0.68	0.71	0.62	0.67	192	0.74	0.78	0.67	0.71
12	0.74	0.78	0.67	0.71	195	0.69	0.73	0.66	0.72
15	0.69	0.73	0.66	0.72	198	0.61	0.70	0.65	0.72
18	0.61	0.70	0.65	0.72	201	0.61	0.70	0.65	0.72
21	0.61	0.70	0.65	0.72	204	0.68	0.72	0.66	0.72
24	0.68	0.72	0.66	0.72	207	0.73	0.78	0.67	0.72
27	0.73	0.78	0.67	0.72	210	0.69	0.73	0.64	0.68
30	0.69	0.73	0.64	0.68	213	0.62	0.65	0.56	0.61
33	0.62	0.65	0.56	0.61	216	0.49	0.52	0.46	0.52
36	0.49	0.52	0.46	0.52	219	0.33	0.40	0.38	0.45
39	0.33	0.40	0.38	0.45	222	0.28	0.39	0.35	0.43
42	0.28	0.39	0.35	0.43	225	0.35	0.41	0.39	0.46
45	0.34	0.41	0.39	0.46	228	0.52	0.54	0.48	0.53
48	0.51	0.53	0.47	0.53	231	0.64	0.66	0.58	0.62
51	0.63	0.66	0.57	0.62	234	0.70	0.74	0.64	0.69
54	0.70	0.74	0.64	0.69	237	0.69	0.74	0.66	0.72
57	0.69	0.74	0.67	0.72	240	0.65	0.74	0.67	0.73
60	0.65	0.74	0.67	0.73	243	0.66	0.73	0.66	0.72
63	0.66	0.73	0.66	0.72	246	0.71	0.73	0.64	0.69
66	0.71	0.74	0.64	0.69	249	0.64	0.66	0.59	0.65
69	0.63	0.66	0.59	0.64	252	0.49	0.57	0.54	0.60
72	0.49	0.56	0.53	0.60	255	0.44	0.56	0.52	0.59
75	0.44	0.55	0.51	0.59	258	0.52	0.58	0.55	0.61
78	0.52	0.57	0.55	0.61	261	0.66	0.69	0.61	0.66
81	0.66	0.68	0.61	0.66	264	0.73	0.76	0.65	0.70
84	0.73	0.76	0.65	0.70	267	0.66	0.71	0.66	0.72
87	0.67	0.72	0.66	0.72	270	0.61	0.71	0.65	0.72
90	0.61	0.71	0.65	0.72	273	0.64	0.70	0.66	0.73
93	0.64	0.70	0.66	0.73	276	0.70	0.75	0.68	0.74
96	0.70	0.75	0.68	0.74	279	0.72	0.79	0.70	0.76
99	0.73	0.79	0.71	0.76	282	0.74	0.77	0.70	0.75
102	0.74	0.78	0.71	0.75	285	0.72	0.75	0.67	0.70
105	0.72	0.74	0.67	0.70	288	0.65	0.66	0.60	0.63
108	0.64	0.66	0.60	0.62	291	0.54	0.55	0.50	0.53
111	0.54	0.55	0.49	0.52	294	0.40	0.42	0.39	0.43
114	0.40	0.42	0.39	0.43	297	0.27	0.33	0.31	0.37
117	0.27	0.33	0.31	0.37	300	0.24	0.32	0.29	0.35
120	0.24	0.32	0.29	0.35	303	0.29	0.34	0.33	0.38
123	0.29	0.34	0.33	0.38	306	0.43	0.45	0.41	0.46
126	0.43	0.45	0.41	0.45	309	0.57	0.58	0.53	0.55
129	0.57	0.58	0.53	0.55	312	0.68	0.69	0.64	0.66
132	0.68	0.69	0.64	0.66	315	0.75	0.77	0.71	0.74
135	0.75	0.77	0.71	0.73	318	0.79	0.83	0.75	0.78
138	0.79	0.83	0.75	0.78	321	0.76	0.80	0.75	0.79
141	0.76	0.80	0.75	0.79	324	0.73	0.80	0.74	0.79
144	0.73	0.80	0.74	0.79	327	0.73	0.78	0.71	0.76
147	0.73	0.78	0.71	0.77	330	0.73	0.75	0.68	0.73
150	0.73	0.75	0.68	0.73	333	0.62	0.67	0.64	0.70
153	0.62	0.67	0.64	0.70	336	0.57	0.66	0.62	0.69
156	0.57	0.66	0.62	0.69	339	0.61	0.67	0.64	0.70
159	0.61	0.67	0.64	0.70	342	0.72	0.74	0.68	0.73
162	0.72	0.74	0.68	0.73	345	0.75	0.81	0.71	0.75
165	0.75	0.81	0.71	0.75	348	0.74	0.78	0.70	0.73
168	0.75	0.79	0.70	0.73	351	0.70	0.72	0.63	0.67
171	0.70	0.72	0.64	0.67	354	0.58	0.60	0.54	0.60
174	0.58	0.60	0.55	0.60	357	0.42	0.49	0.46	0.53
177	0.42	0.49	0.47	0.54	360	0.36	0.47	0.43	0.51
180	0.36	0.47	0.43	0.51					

180°), which also show very low efficiencies. As observed at Horns Rev I, it is interesting to see that for these highly wake-affected sectors the results using the direction uncertainty show higher efficiencies (compared to the $\sigma = 0^\circ$ cases), whereas for those sectors with general higher efficiencies, both cases (with and without uncertainty) show similar efficiencies as the uncertainty ones just slightly account for directions where the wake is highest.

5 Summary and conclusions

Simulations of power deficits were carried out using a modified version of the Park wake model used. The model estimates the wind speed deficit (and thus relates to the power deficit through the power curve) taking into account the free wind speed, distance between turbines, turbine's diameter and thrust, and the wake decay coefficient (or wake expansion). The latter was related to roughness, atmospheric stability and turbulence and so the model can be used in a variety of wind conditions.

In order to compare the results of the model with the data, we performed post-processing of the model simulations accounting (or not) for the uncertainty in the wind direction as the data (averaged over a range of wind directions) come from SCADA power data averaged over a typical time interval of 10-min. Further uncertainties due to the variability of wind within the wind farm and turbine's yaw misalignments (among others) are inherently present in the data.

The simulations agree very well with the observations at Horns Rev I, particularly when we post-processed the simulation results to partly take into account the wind direction uncertainty. There is also better agreement between simulations and observation when the wake decay coefficient is estimated either as function of the roughness, height, and atmospheric stability or turbulence intensity. For Lillgrund the results are not as good as those found at Horns Rev I (at least with this analysis of the observations). The trends of the simulations and the the observations are generally the same. When the direction uncertainty is taken into account, the simulations become closer to the observations. When parameterizing the wake decay coefficient, we also find a closer agreement between simulations and observations.

Acknowledgments

Data from the Horns Rev I and the Lillgrund wind farms are kindly provided by DONG Energy and Vattenfall. Funding from the EERA DTOC contract FP7-ENERGY-2011/no.282797 and the IEA-WakeBench research collaboration project are also acknowledged.

References

Frandsen, S., 1992: On the wind speed reduction in the center of large clusters of wind turbines. *Journal of Wind Engineering and Industrial Aerodynamics*, **39**, 251–265.

Gaumond, M., P.-E. Rethoré, S. Ott, A. Peña, A. Bechmann, and K. S. Hansen, 2013: Evaluation of the wind direction uncertainty and its impact on wake modelling at the Horns Rev offshore wind farm. *Wind Energy*, in press.

Hansen, K., 2013a: WP1 wake model performance validation results for horns rev offshore wind farm. Tech. Rep. Technical report for the EERA-DTOC project, DTU Wind Energy.

Hansen, K., 2013b: WP1 wake model performance validation results for lillgrund offshore wind farm. Tech. Rep. Technical report for the EERA-DTOC project, DTU Wind Energy.

Hansen, K. S., R. J. Barthelmie, L. E. Jensen, and A. Sommer, 2012: The impact of turbulent intensity and atmospheric stability on power deficits due to wind turbine wakes at horns rev wind farm. *Wind Energy*, **15**, 183–196.

Jensen, N. O., 1983: A note on wind generator interaction. Tech. Rep. Risoe-M-2411(EN), Risø National Laboratory, 16 pp.

Katic, I., J. Højstrup, and N. O. Jensen, 1986: A simple model for cluster efficiency. *Proceedings of the European Wind Energy Association Conference & Exhibition*, Rome.

Monin, A. S. and A. M. Obukhov, 1954: Osnovnye zakonomernosti turbulentnogo peremeshivanija v prizemnom sloe atmosfery (Basic laws of turbulent mixing in the atmosphere near the ground). *Trudy Geofiz. Inst. AN SSSR*, **24 (151)**, 163–187.

Mortensen, N. G., D. N. Heathfield, L. Myllerup, L. Landberg, and O. Rathmann, 2007: Getting started with WAsP 9. Tech. Rep. Risø-I-2571(EN), Risø National Laboratory, Roskilde, Denmark, *http:/www.wasp.dk/Download/DownloadFiles/General/Getting Started with WAsP 9.pdf*.

Panofsky, H. A. and J. A. Dutton, 1984: *Atmospheric turbulence*. John Wiley & Sons, 397 pp pp.

Peña, A., 2009: Sensing the wind profile. Tech. Rep. Risø-PhD-45(EN), Risø DTU, 80 pp.

Peña, A. and S.-E. Gryning, 2008: Charnock's roughness length model and non-dimensional wind profiles over the sea. *Boundary-Layer Meteorol.*, **128**, 191–203.

Peña, A., S.-E. Gryning, and C. B. Hasager, 2008: Measurements and modelling of the wind speed profile in the marine atmospheric boundary layer. *Bound.-Layer Meteorol.*, **129**, 479–495.

Peña, A. and A. N. Hahmann, 2012: Atmospheric stability and turbulent fluxes at Horns Rev–an intercomparison of sonic, bulk and WRF model data. *Wind Energy*, **15**, 717–730.

Peña, A., C. B. Hasager, S.-E. Gryning, M. Courtney, I. Antoniou, and T. Mikkelsen, 2009: Offshore wind profiling using light detection and ranging measurements. *Wind Energy*, **12**, 105–124.

Peña, A. and O. Rathmann, 2013: Atmospheric stability dependent infinite wind farm models and the wake decay coefficient. *Wind Energy*, in press.

Peña, A., P.-E. Réthoré, and O. Rathmann, 2013: Modeling large offshore wind farms under different atmospheric stability regimes with the park wake model.

DTU Wind Energy
Technical University of Denmark

Frederiksborgvej 399
4000 Roskilde
Denmark
Phone +45 4677 5024

www.vindenergi.dtu.dk